How to cite: *Angew. Chem. Int. Ed.* **2026**, e26135
doi.org/10.1002/anie.202526135

Radical Chemistry

Where Enantioselection is Set: A Mechanistic Framework for Asymmetric Hydrogen-Atom Transfer

Zhongyun Xu[+], *Yufeng Yang*[+], *and Yong-Qiang Zhang**

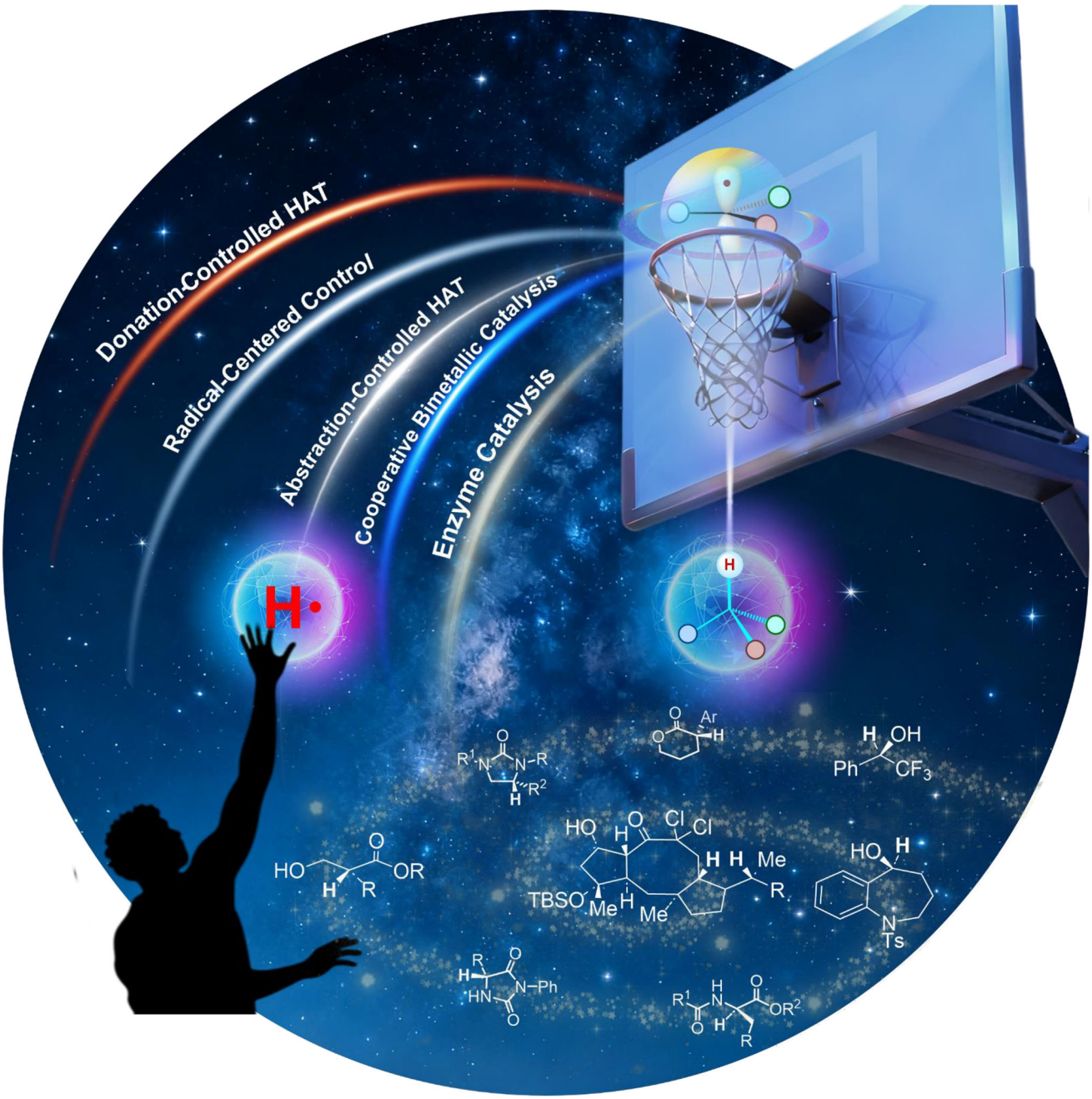

Angewandte International Edition Chemie

Abstract: Hydrogen-atom transfer (HAT) lies at the heart of radical chemistry, yet asymmetric HAT has been difficult because the high reactivity of radicals often forces H-transfer to proceed through early, weakly organized transition states, yielding small $\Delta\Delta G^{\ddagger}$ and allowing rapid racemic background pathways to compete. Recent advances across small-molecule, metalloradical, cooperative, peptide, and enzymatic catalysis show that high enantioselectivity is attainable when the catalyst is engineered to exert stereocontrol precisely at the H-transfer step that sets configuration. In this minireview, we organize asymmetric HAT into five regimes—donation-controlled termination, radical-centered control, abstraction-controlled HAT, cooperative bimetallic catalysis, and enzyme-mediated HAT—each specified by where chiral information is introduced during H-transfer. Through representative cases, we illustrate how catalysts achieve enantioselection by defining radical geometry, guiding H-delivery, enforcing selective hydrogen abstraction, or confining donor–acceptor pairs within organized chiral environments. This mechanistic framework provides a unified lens spanning synthetic and biocatalytic systems, clarifies the distinct stereochemical logics in each regime, and highlights emerging opportunities for expanding asymmetric radical chemistry through precisely orchestrated H-atom transfer.

1. Introduction

Hydrogen-atom transfer (HAT)—the movement of H• between two partners—is one of the most adaptable elementary steps in radical chemistry.[1–3] It can initiate, propagate, or terminate radical processes and operates under thermal, photochemical, electrochemical, and enzymatic conditions.[4–8] By regulating how substrates enter radical manifolds or how radicals are ultimately quenched, HAT supports a wide range of valuable transformations, including C─H functionalization, hydrofunctionalization of alkenes, reductive and redox-neutral events, and isotopic labeling.[9,10] Its broad presence in both synthetic and biological systems underscores HAT as a deeply conserved and versatile mode of reactivity.

Despite this prevalence, achieving enantioselective HAT has long been challenging. Radicals engage in fast, low-barrier reactions, and H-transfer typically proceeds through early, weakly organized transition states that offer only small $\Delta\Delta G^{\ddagger}$ between competing pathways.[11,12] Under such circumstances, racemic background reactions readily compete. Effective stereocontrol, therefore requires catalysts capable of introducing chiral influence at the precise moment of H-atom transfer—whether by preorganizing a prochiral radical, tuning the donor environment, or directing the trajectory of a hydrogen-abstraction event. Over the past four decades, the development of well-defined chiral donors, templating environments, cooperative manifolds, peptide-based catalysts, and enzymatic systems has shown that HAT can indeed serve as a reliable stereodefining step.

Positioning Within the Existing Literature. Several prior reviews have addressed aspects of HAT chemistry, including broad surveys of radical C─H functionalization,[13–20] summaries of metal-catalyzed hydrofunctionalization,[21–23] and early accounts of asymmetric HAT.[24,25] These studies highlighted key reaction classes, catalyst families, and synthetic opportunities. Building on this foundation, the present Minireview adopts a mechanistic perspective with an emphasis on how and where enantioselection is introduced in H-atom transfer. Whereas earlier method-focused discussions typically organize examples by catalyst type, donor class, or activation mode,[26–28] our approach centers on a unifying question—"Where is enantioselection set?"—which enables direct comparison between fundamentally different stereodetermining events. This framework incorporates all major modes of asymmetric HAT, including donor-controlled, radical-centered, abstraction-controlled, and enzyme-based regimes, and also highlights newly emerging homocooperative bimetallic architectures. Framing the field in this way clarifies the stereochemical logic operating in each regime and reveals conceptual connections that are not apparent from catalyst- or method-based classifications.

Mechanistic Classification Framework. Five mechanistic settings emerge from this analysis (Figure 1a):

i) Donation-controlled termination, in which a chiral H-donor—either pre-formed or generated in situ—governs facial selectivity during radical quenching.
ii) Radical-centered control, where the radical is positioned within a chiral pocket, such as a Lewis acid or hydrogen-bonding scaffold, before accepting hydrogen-atom from an achiral donor.
iii) Abstraction-controlled HAT, in which stereocontrol arises during hydrogen-atom abstraction at the radical-generation stage, enabling kinetic resolution or desymmetrization of the starting material.
iv) Cooperative bimetallic platforms, which activate both donor and acceptor within a homocooperative bimetallic chiral environment, coordinating X–H bond weakening and substrate activation to enforce a unified H-transfer geometry.
v) Enzymatic Asymmetric HAT, where NADPH- and FMN-dependent reductases deliver hydrogen-atom with precise facial selectivity under either ground-state or photoactivated conditions.

Although these approaches differ in catalyst architecture and activation mode, they share a central principle: effective asymmetric HAT requires a well-organized microenvironment at the instant of H-transfer, ensuring that the chiral pathway dominates over nonselective alternatives.

[*] Z. Xu[+], Y. Yang[+], Y.-Q. Zhang
School of Chemistry and Chemical Engineering, Shandong University, Jinan 250100, China
E-mail: yongqzhang@sdu.edu.cn
[+] Both authors contributed equally to this work.

The representative examples that follow illustrate how various catalyst platforms achieve such organization—through confinement, polarity matching, orchestrated radical generation, or cofactor-guided H-delivery.

Terminology. Throughout this review, we use the following terminology: HAT (hydrogen-atom transfer), HAA (hydrogen-atom abstraction), SET (single-electron transfer), PCET (proton-coupled electron transfer), PRC (polarity-reversal catalysis), BDE (bond dissociation energy), KIE (kinetic isotope effect), and AIBN (azobisisobutyronitrile). For biocatalysis, ERED, KRED, and IRED denote ene-, keto-, and imine-reductases; NADPH is the hydride-donating nicotinamide cofactor used by reductases, while FMN, FMN_{sq}, and FMN_{hq} denote the oxidized, semiquinone, and fully reduced states of flavin mononucleotide that mediate SET and HAT steps in flavoprotein catalysis. EDA complexes are ground-state donor-acceptor assemblies that enable photochemical activation through photoinduced electron transfer.

Scope and Purpose. A survey of the literature illustrates the evolving nature of asymmetric HAT (Figure 1b): donation-controlled systems dominated early developments, followed by the emergence of radical-centered and abstraction-controlled approaches. In recent years, enzymatic HAT has expanded rapidly, while cooperative architectures have opened new opportunities for integrating radical generation and stereocontrolled termination within a single organized framework.

Figure 1b does not represent an exhaustive bibliometric analysis of all asymmetric HAT reports. Instead, it is constructed from the curated set of representative studies discussed in this Minireview. These references were selected to i) capture historically formative contributions, ii) exemplify each mechanistic regime with clear stereochemical logic, and iii) reflect recent conceptual and methodological advances. The resulting distribution therefore visualizes the mechanistic and temporal balance of the field as framed by the present review, rather than the absolute publication volume in each period.

This minireview is not intended to provide exhaustive coverage of enantioselective HAT. In particular, enzyme-catalyzed HAT is a rapidly emerging field whose breadth makes comprehensive treatment impractical. Instead, we focus on outlining the practical mechanistic features that define each mode of enantioselection and discussing representative examples that illustrate these principles in action.

Our aim is both tutorial and forward-looking. We highlight emerging directions such as cooperative redox catalysts, tunable and sustainable hydrogen donors, and new photochemical and electrochemical activation modes. By articulating the mechanistic logic that underpins stereocontrol in H-atom transfer, we hope to provide practical design guidelines that can inform the development of next-generation asymmetric HAT transformations—ones that achieve high levels of stereocontrol, operate under greener and more sustainable conditions, and translate reliably to complex and functionally rich molecular settings.

Zhongyun Xu received her B.S. degree from Jiangsu Normal University in 2019. and obtained her MS degree in 2022 from Shandong University under the supervision of Professor Yong-Qiang Zhang. She is currently a PhD student in the same group, focusing on asymmetric hydrogen-atom transfer reactions and the development of novel hydrogen-atom donors.

Yufeng Yang is a research assistant in Prof. Yong-Qiang Zhang's group at Shandong University, he contributes to projects in transition metal catalysis, demonstrating strong academic potential and a dedicated interest in organic chemistry, especially catalytic methods. Beyond research, he enjoys running and reading, reflecting a well-rounded personal life.

Yong-Qiang Zhang earned his B.S. and Ph.D. from Lanzhou University under the mentorship of Professor Yong-Qiang Tu. After a brief research stint at Georgia State University, he won a Humboldt postdoctoral fellowship in Professor Andreas Gansäuer's group at the Kekulé-Institute, University of Bonn. Subsequently, he pursued another postdoctoral position in Professor Christa Müller's group at the university's pharmaceutical institute before joining Shandong University in 2019. His current research interests are asymmetric titanium radical catalysis and the synthesis of bioactive natural products.

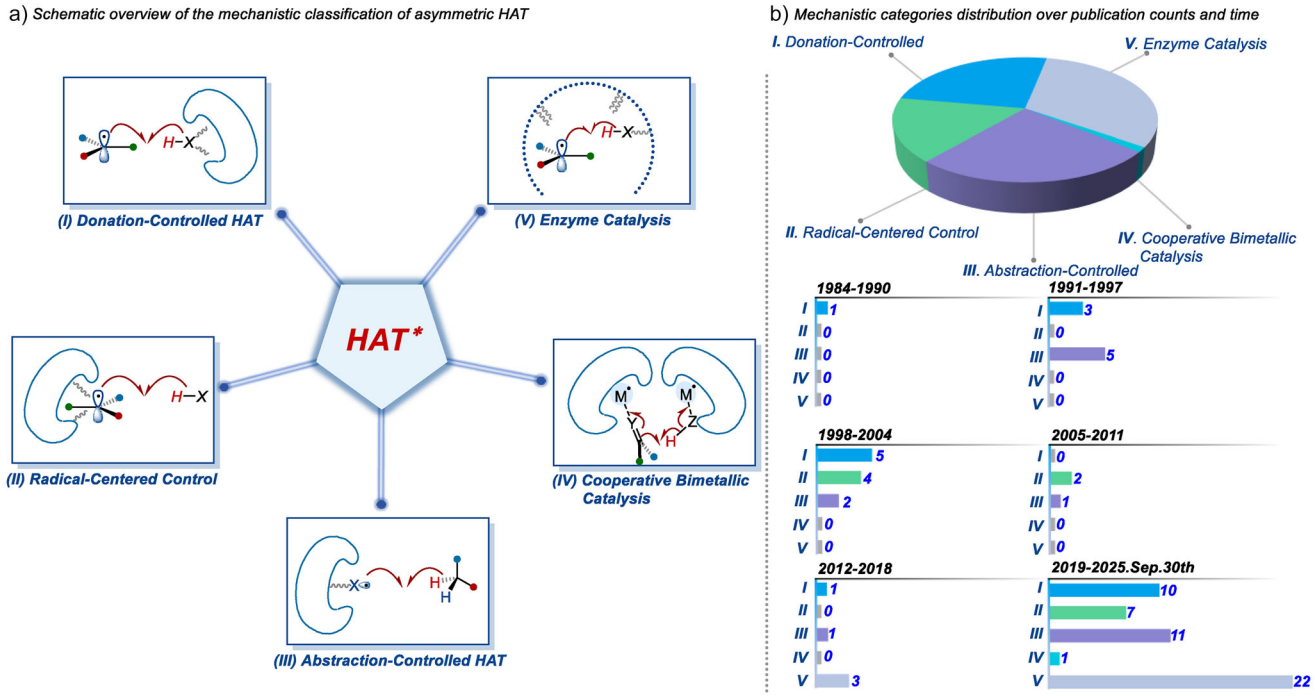

Figure 1. Mapping asymmetric HAT: Mechanistic classification and development trends. a) Schematic overview of the mechanistic classification of asymmetric HAT. b) Mechanistic categories distribution over publication counts and time.

2. Donation-Controlled Termination

In donation-controlled systems, enantioselectivity is imparted by a chiral hydrogen-atom donor that transfers H• to a prochiral radical. This approach represents the most intuitive entry to asymmetric HAT and has been developed through both pre-formed donor molecules and in-situ generated donors.

2.1. Stoichiometric Pre-Formed Chiral H-Donors

2.1.1. Dihydronicotinamides

The first attempts to achieve asymmetric HAT relied on stoichiometric chiral donors. In a landmark study (Scheme 1),[29] Tanner drew inspiration from nature's NADPH cofactor and prepared a chiral 1,4-dihydronicotinamide **NAM-1** to reduce trifluoroacetyl ketyl radical **3**. The reaction operated as a radical chain: AIBN initiated HAA from dihydronicotinamide **NAM-1** to generate the chiral nicotinyl radical **NAM•**. This radical transferred a single electron to trifluoroacetophenone, generating the ketyl radical anion **3** while oxidizing itself to the corresponding pyridinium salt **NAM$^+$**. Subsequent enantioselective HAT from **NAM-1** to **3** yielded the reductive product **2**. Despite modest enantioselectivity (68% *ee*) and a very limited substrate scope, this study provided the first compelling evidence that embedding chirality within the hydrogen-atom donor can enforce stereocontrol in the radical asymmetric HAT.

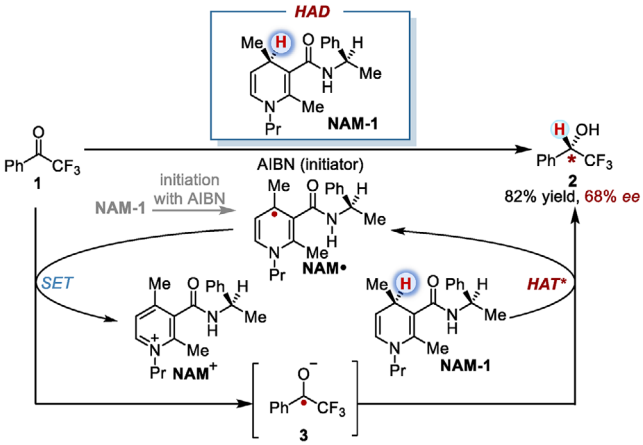

Scheme 1. Pioneering asymmetric HAT with a chiral NADPH-inspired dihydronicotinamide donor (Tanner, 1988).

2.1.2. Stannanes

Building on this proof of principle, researchers turned to organotin hydrides, long established as highly efficient hydrogen-atom donors owing to the low BDE of the Sn–H bond.[30] Within this context, homolytic reductive dehalogenation of racemic α-bromo carbonyl compounds proves to be an ideal model platform, undergoing a radical chain process involving sequential halogen-atom abstraction and HAT reaction (Scheme 2a). Several tin hydrides incorporating chiral frameworks have been applied to impart enantiocontrol in the HAT processes. Curran's group reported the first chiral tin hydride **Sn-1** (Scheme 2b),[31] featuring an axially chiral

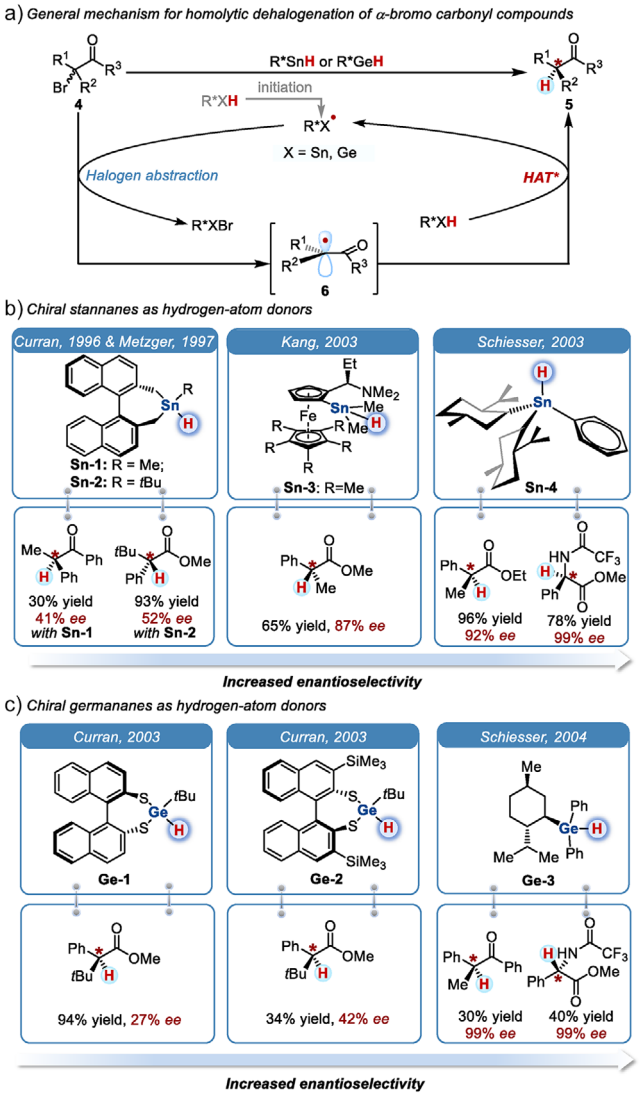

Scheme 2. Chiral stannanes and germanes as stoichiometric hydrogen-atom donors for asymmetric HAT. a) General mechanism for homolytic dehalogenation of α-bromo carbonyl compounds. b) Chiral stannanes as hydrogen-atom donors. c) Chiral germananes as hydrogen-atom donors.

binaphthyl backbone, which reduced α-bromo aryl ketones to form α-tertiary stereocenters with moderate *ee* (41%). Metzger enhanced the steric environment by introducing ortho-tert-butyl substituents to generate **Sn-2** (Scheme 2b),[32] which reduced α-bromoesters to afford the reduction product in slightly higher *ee* (52%), underscoring steric bias as the primary source of enantiodifferentiation. Notably, this scaffold also enabled a catalytic variant in which the tin hydride was regenerated in situ with $NaBH_3CN$ without erosion of stereocontrol. Kang's group advanced the design by developing a ferrocene-based tin hydride **Sn-3** (Scheme 2b), where an amino substituent on the Cp ring coordinated to the tin center to rigidify the geometry, resulting in satisfactory stereoselectivity (87% *ee*) in the reduction of 2-bromo-2-phenylpropanoate.[33] In parallel, Schiesser synthesized a C_2-symmetric stannane **Sn-4** bearing two menthyl groups (Scheme 2b), which—under $MgBr_2$ activation—reduced α-bromoesters in a radical chain process to give products with excellent enantioselectivity (99% *ee*), establishing a benchmark for stoichiometric tin-based HAT reagents.[34]

Germanes: Given the intrinsic toxicity and difficult purification associated with organotin hydrides, the search for safer, more sustainable HAT donors naturally turned toward germanium hydrides as promising alternatives. In 2003, Curran and co-workers pioneered the development of the first chiral germanium-based donor **Ge-1**,[35] built on an axially chiral binaphthyl scaffold (Scheme 2c). When applied to the homolytic reduction of α-bromoesters, **Ge-1** delivered high conversions but disappointingly low enantioselectivity. To improve stereocontrol, Curran's group further designed **Ge-2**,[35] introducing ortho-trimethylsilyl substituents onto the binaphthyl framework to increase steric bias. This modification indeed enhanced enantioselectivity but at a significant cost: overall reactivity and isolated yield dropped sharply, highlighting the delicate trade-off between steric crowding (needed for asymmetric induction) and the intrinsic reactivity of Ge–H bonds in radical chain processes.

Following these efforts, Schiesser and co-workers (2004) introduced **Ge-3** (Scheme 2c),[36] a chiral germane featuring menthyl and phenyl substituents. In a pivotal study, they demonstrated that with a Lewis acid co-catalyst ($MgBr_2$), **Ge-3** delivered excellent enantioselectivities across a broad substrate scope—including α-bromoketones, α-bromoesters, and amino acid derivatives.

2.2. Catalytic Pre-Formed Donors: Chiral Thiols

Having established that chirality embedded in the hydrogen-atom donors can effectively bias radical termination, efforts naturally shifted toward developing catalytic HAT donors that are safer, more sustainable, and more synthetically versatile than stoichiometric stannanes or germanes. Chiral thiols emerged as an ideal solution: The S–H bond has a relatively low BDE, enabling facile HAT, and the thiol functionality is modular, allowing precise tuning of both steric environment and electronic properties. Recent advances can be categorized into three mechanistically distinct yet complementary classes: i) PRC–enabled chiral thiols, which harness polarity matching to accelerate and enantiocontrol HAT; ii) peptide-scaffolded thiols, which leverage secondary-structure preorganization and hydrogen-bonding networks to achieve high stereocontrol under photoredox conditions; and iii) rigid small-molecule thiol scaffolds—particularly C_2-symmetric arylthiols—which provide modular, readily tunable steric and electronic environments and deliver high levels of enantiocontrol when combined with photoredox catalysis.

2.2.1. Polarity-Reversal Catalysis with Chiral Thiols

A major conceptual breakthrough came with PRC, introduced by Roberts in 1999,[37,38] In radical H-abstraction, rates and selectivities depend strongly on polar effects:

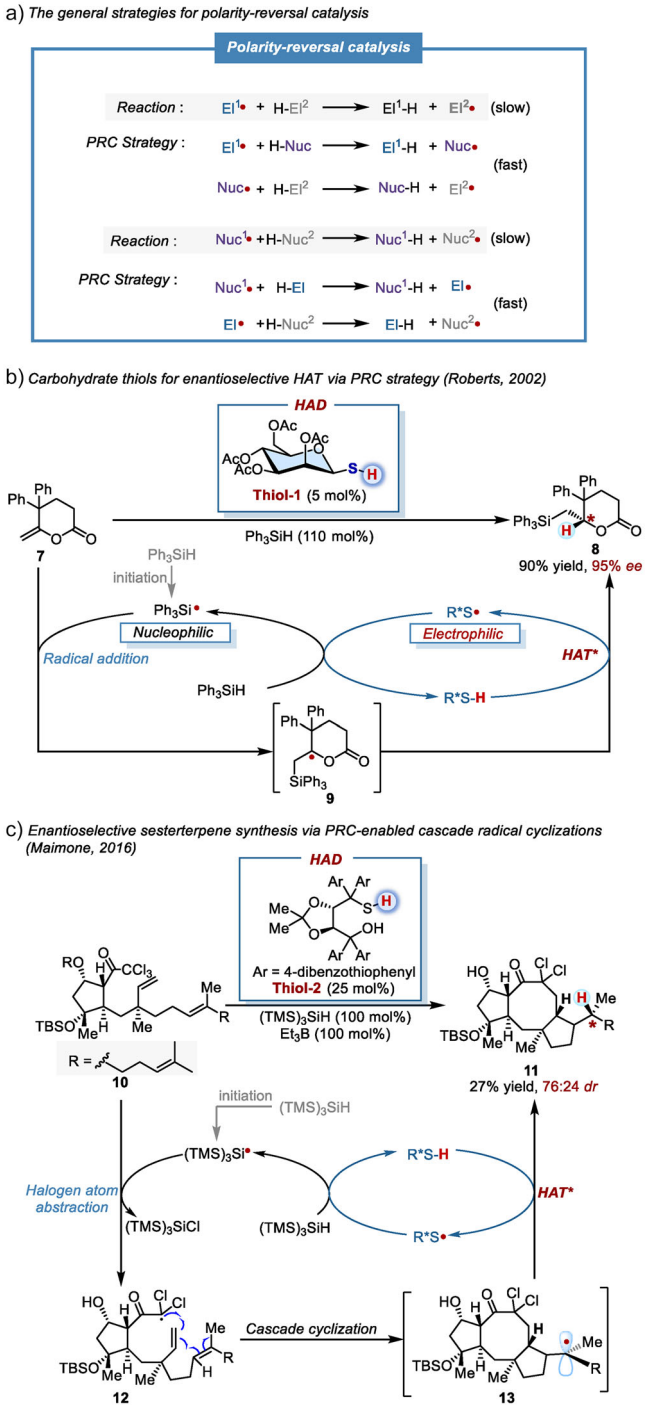

Scheme 3. PRC-enabled chiral thiol catalysis for asymmetric HAT. a) The general strategies for PRC. b) Carbohydrate thiols for enantioselective HAT via PRC strategy. c) Enantioselective sesterterpene synthesis via PRC-enabled cascade radical cyclizations.

electrophilic radicals abstract H• faster from electron-rich C–H bonds, while nucleophilic radicals prefer electron-poor sites (Scheme 3a). PRC turns a polarity-mismatched, sluggish single-step HAT into a low-barrier, two-step process by generating radicals of opposite polarity to match the substrate. This simple yet powerful idea provided a general strategy to accelerate and control HAT. This concept enabled the first catalytic asymmetric HAT: the radical-chain hydrosilylation of methylenelactones **7** mediated by carbohydrate-derived chiral thiol (**Thiol-1**) (Scheme 3b).[39] Mechanistically, the catalytic cycle begins with homolysis of di-tert-butyl hyponitrite (TBHN) to generate *t*BuO•, which abstracts H• from triphenylsilane, forming a nucleophilic silyl radical Ph_3Si•. This radical adds to the electron-deficient olefin moiety of **7** to generate carbon-centered radical **9**, which undergoes enantioselective HAT from the chiral thiol. This step simultaneously forms an electrophilic thiyl radical, which is rapidly reduced by the silane to close the catalytic cycle. Remarkably, the combination of stoichiometric phenylsilane and catalytic glucose-derived chiral thiol provided both high reactivity and excellent enantioselectivity, establishing catalytic donor-controlled HAT as a practical asymmetric strategy.

Building on this conceptual foundation, Maimone and co-workers elegantly applied the PRC approach to the total synthesis of (–)-6-epi-ophiobolin N, a complex sesterterpene natural product (Scheme 3c). The key step was a cascade radical cyclization that rapidly assembled the[5,8,5] tricyclic skeleton **11** with excellent diastereoselectivity. The sequence begins with halogen-atom abstraction to form radical intermediate **12**, followed by a cascade cyclization to give tertiary carbon radical **13**, which undergoes enantioselective HAT from the chiral thiol (**Thiol-2**).[40] Extensive screening identified TADDOL-derived chiral thiols as optimal, delivering the desired stereochemistry in the HAT step. This application showcased the power of PRC-assisted thiol catalysis to enable concise access to complex terpene frameworks and highlighted its applicability for radical cyclizations and natural product synthesis.

2.2.2. Peptide-Scaffolded Thiols

The integration of chiral peptide thiols with visible-light photoredox catalysis and PCET manifolds has driven a surge of innovation in asymmetric HAT, offering powerful tools for deracemization, hydrofunctionalization of olefins, and isotope labeling under mild conditions (Figure 2). These systems leverage the conformational rigidity of β-turn peptide scaffolds to preorganize the thiol relative to the radical intermediate, allowing well-defined HAT transition states and high enantioselectivity.

The breakthrough came from Knowles and Miller, who reported the deracemization of cyclic ureas via a light-driven sequential PCET/HAT process (Scheme 4a),[41] The reaction begins with oxidation of the urea substrate **14** by photoexcited Ir(III), generating a nitrogen-centered radical cation **15**. Stereoselective deprotonation by a chiral phosphate converts (*S*)-**15** preferentially into neutral radical **16**, whereas (*R*)-**15** undergoes back electron transfer with Ir(II) to regenerate (*R*)-**14**.

Radical **16** is then captured by enantioselective HAT from a cysteine-containing tetrapeptide thiol (**Thiol-3**), delivering (*R*)-**14**. Two discrete stereocontrolling steps—proton transfer by the chiral phosphate and peptide-thiol-mediated HAT—together enable full deracemization, establishing a

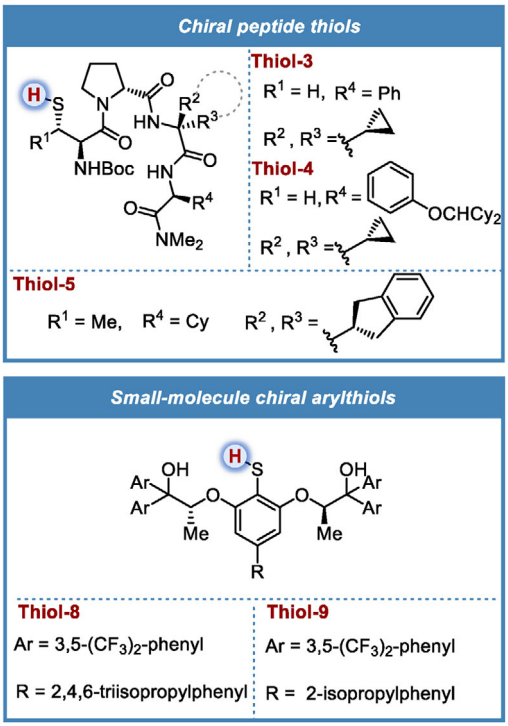

Figure 2. Peptide-scaffolded thiols and small-molecular chiral arylthiols.

conceptual blueprint for multi-catalytic asymmetric radical processes. Subsequently, the same research group developed an asymmetric radical hydroamination of alkenes with sulfonamides (Scheme 4b). The mechanism proceeds through light-driven N–H PCET of **17** to generate amidyl radical **20**, which undergoes anti-Markovnikov addition to the olefin **18**, followed by enantioselective HAT from the tetrapeptide thiol (**Thiol-4**, shown in Figure 2).[42] Mechanism experiment and DFT calculations revealed a cooperative interplay of hydrogen bonding, $\pi-\pi$ stacking, and London dispersion interactions between the radical intermediate and the chiral pocket, offering detailed insight into the subtle interactions governing stereoselectivity in HAT.

Most recently, Knowles and co-workers expanded this strategy to the enantioselective hydrodifluoroalkylation of alkenes (Scheme 4c).[43] Upon visible-light excitation, the Ir(III) catalyst engages in oxidative quenching with bromodifluoroamide **22**, generating difluoroamide radical **25**, which adds anti-Markovnikov to the enol ester **23**, producing prochiral radical **26**. The enantiodetermining HAT then occurs within the β-turn-biased structure pocket of the peptide catalyst, directed by a key hydrogen bond between the amide carbonyl and the Aic (2-aminoindane-2-carboxylic acid) N–H residue, furnishing the product **24** in high *ee*.

Ye and co-workers pushed the platform toward isotopic labeling, particularly deuterium incorporation. In 2022, they reported the enantioselective deuterofunctionalization of methylenelactams and methylenelactones **28** (Scheme 5a).[44] D_2O served as the ultimate deuterium source in the deuterium atom transfer (DAT) step to the prochiral carbon radical. Mechanistic studies revealed that D_2O also partic-

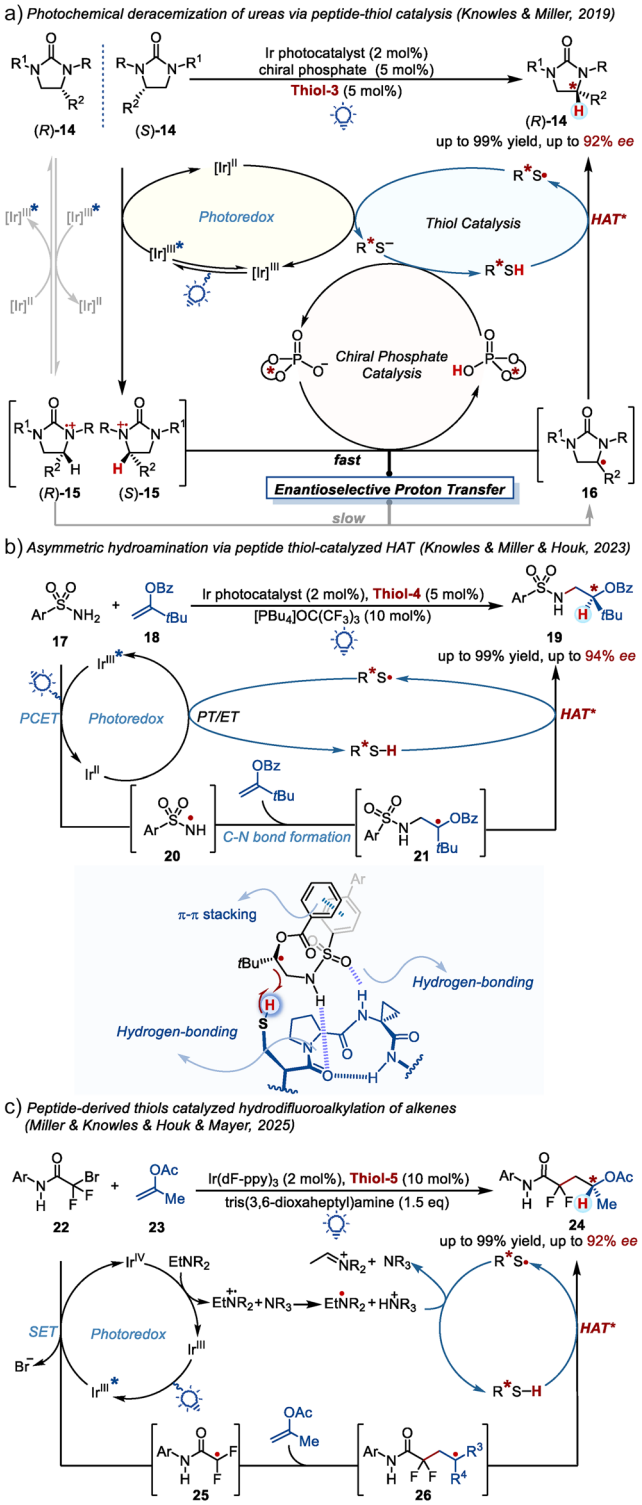

Scheme 4. Peptide-thiol catalysis in asymmetric HAT: deracemization and hydrofunctionalization strategies. a) Photochemical deracemization of ureas via peptide-thiol catalysis. b) Asymmetric hydroamination via peptide thiol-catalyzed HAT. c) Peptide-derived thiols catalyzed hydrodifluoroalkylation of alkenes.

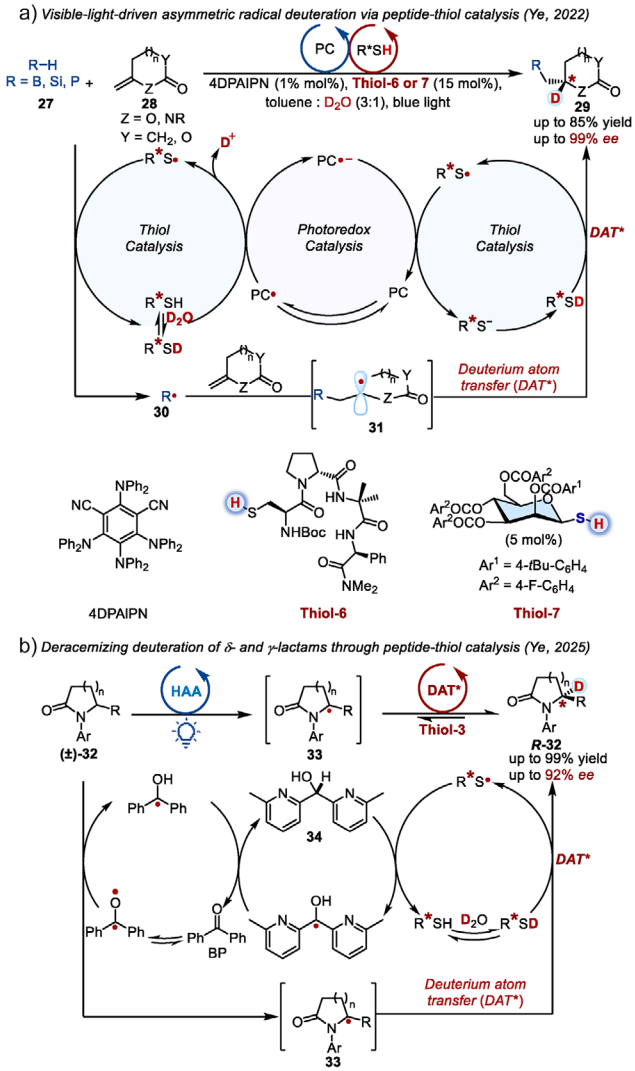

Scheme 5. Asymmetric deuterium incorporation via peptide-thiol HAT platforms. a) Visible-light-driven asymmetric radical deuteration via peptide-thiol catalysis. b) Deracemizing deuteration of δ-and γ-lactams through peptide-thiol catalysis.

ipated in the initial step by acting as a proton acceptor in a concerted PCET process, which facilitated the efficient generation of the thiyl radical catalyst and enhanced the reaction rate. This synergistic dual role of D_2O, combined with the enantiofacial control exerted by the chiral thiol catalyst, enabled the highly enantioselective construction of non-benzylic deuterated stereocenters.

In a subsequent development, Ye's group reported a dual-HAT strategy that combined benzophenone (BP) as a nonselective H-atom abstractor with the peptide thiol as the enantioselective donor (Scheme 5b).[45] Upon photoexcitation, BP abstracts H• from either enantiomer of racemic lactams (±)-**32** to generate prochiral radical **33** and a benzophenone ketyl radical. Enantiodetermining HAT from the tetrapeptide thiol (**Thiol-3**) —preorganized by hydrogen bonding and steric fit—then sets the stereocenter. Based on the mechanistic studies, the bis(6-methylpyridin-2-yl)methanol additive **34** functions as an electron and hydrogen-atom shuttle to facilitate the turnover of BP and the **Thiol-3**. This dual activation mode enabled simultaneous deracemization and deuteration (>95% D incorporation) of N-aryl δ-alkyl lactams and gave concise access to deuterated alkaloids such as d_1-norbgugaine.

Taken together, these studies chart the rapid maturation of peptide-thiol scaffolds from a conceptual curiosity to a robust and modular platform for enantioselective radical termination. By uniting secondary-structure preorganization, PCET-driven radical generation, and photoredox turnover, this strategy now supports transformations ranging from deracemization to hydrofunctionalization and efficient isotopic labeling.

2.2.3. Small-Molecule Chiral Arylthiols

Complementary to peptide-based catalysts, small-molecule chiral arylthiols have recently emerged as powerful HAT donors that achieve stereocontrol through rigid C_2-symmetric frameworks. These catalysts provide tunable steric and electronic environments, making them attractive for streamlined reaction development.

A seminal contribution came from Dong and co-workers, who designed a C_2-symmetric thiophenol catalyst derived from lactate ester and applied it to an intramolecular hydroamination reaction under photoredox conditions (Scheme 6a). This photocatalytic enantioselective hydroamination proceeds through oxidation of the alkene **35** to a cation radical **37**, which undergoes cyclization to form a prochiral carbon-centered radical **38**. The enantiodetermining step is a HAT from **Thiol-8**, affording 3-substituted piperidines **36** in high *ee*.[46]

Expanding this approach, Dong's group reported an enantioconvergent decarboxylative HAT platform that merges photoredox catalysis for radical generation with arylthiol catalysis for enantiocontrolled reductive radical termination (Scheme 6b).[47] Upon photoexcitation, the photocatalyst (Mes–Acr$^+$–Ph) oxidizes indoline-3-carboxylic acid **40** to generate a carboxyl radical **42**, which rapidly decarboxylates to yield a tertiary prochiral radical **43**. The key stereodetermining event is HAT from the chiral arylthiol (**Thiol-9**), with DFT calculations indicating that facial selectivity is enforced by π–π interactions between its 3,5-$(CF_3)_2C_6H_3$ moiety and the substrate's benzyl group. The resulting thiyl radical is then reduced by Mes–Acr–Ph* to regenerate the active thiol catalyst, completing the cycle and delivering enantioenriched indoline products in high *ee*.

2.3. In Situ-Generated Chiral H-Donors

Beyond pre-synthesized donors, an alternative strategy is to assemble the chiral hydrogen-atom donor directly in situ under catalytic conditions, thereby avoiding donor preparation and expanding the range of reactive species available. In 2024, Li and co-workers reported an elegant approach based on an in situ generated chiral 8H-BINOL/decatungstate complex (**Cat-1/DTs**) (Scheme 7a).

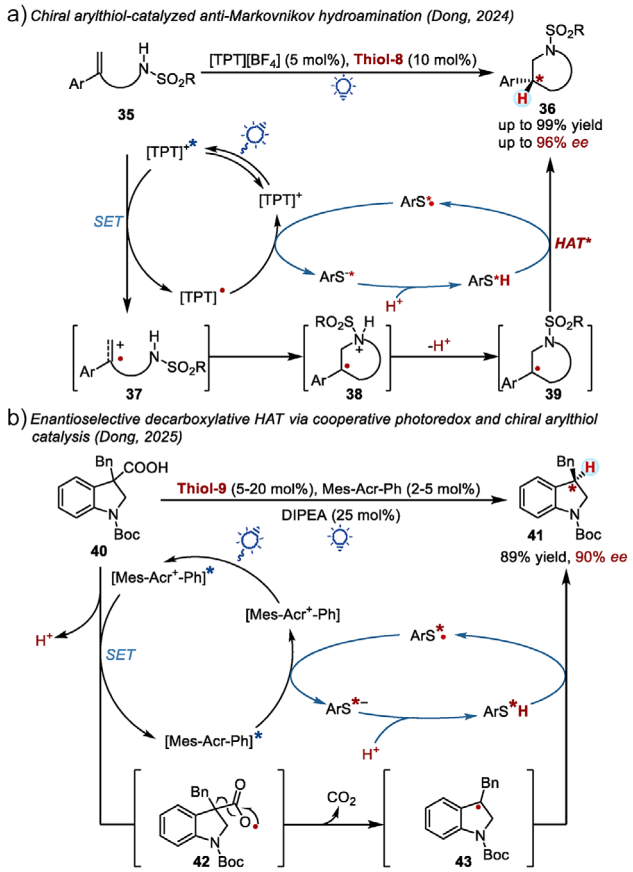

Scheme 6. Chiral arylthiol catalysts for enantioselective hydroamination and decarboxylative HAT. a) Chiral arylthiol-catalyzed anti-Markovnikov hydroamination. b) Enantioselective decarboxylative HAT via cooperative photoredox and chiral arylthiol catalysis.

Sterically tuned 8H-BINOL (**Cat-1**) is deprotonated by K_2CO_3 to form an aryloxide (ArO^-), then with **TBADT**. Upon UV excitation, the resulting chiral **Cat-1/DTs*** complex abstracts hydrogen from unactivated aliphatic C(sp^3)—H bonds in cyclohexane to form a cyclohexyl radical and a reduced **Cat-1/DTs-H*** species. Critically, **Cat-1/DTs-H*** then acts as the chiral H-atom donor, delivering hydrogen to the prochiral carbon radical **47** (e.g., generated by radical addition to vinylpyridines **44**) through a sterically organized transition state. This design conceptually transforms a well-known HAT photocatalyst (decatungstate) into a chiral, self-assembled donor with high enantioselectivity.[48]

Feng and co-workers introduced a complementary system built from a photoexcited quinone coordinated to a chiral Pr(III)/N, N′-dioxide Lewis acid (Scheme 7b). Visible-light excitation of the quinone generates a semiquinone radical (**PQ-H•**), which—held within the chiral Lewis acid pocket—abstracts hydrogen from an ether ring (C—H BDE ≈ 86–99 kcal mol^{-1}) to form an alkyl radical. The radical then adds to a Pr(III)-activated acrylamide, generating an α-carbonyl radical **51** that subsequently undergoes stereocontrolled back-HAT from **PQ-H•**, regenerating the quinone and setting the stereocenter in product **50**. KIE (3.1) confirmed HAT as rate-determining step, and DFT calculations revealed that the

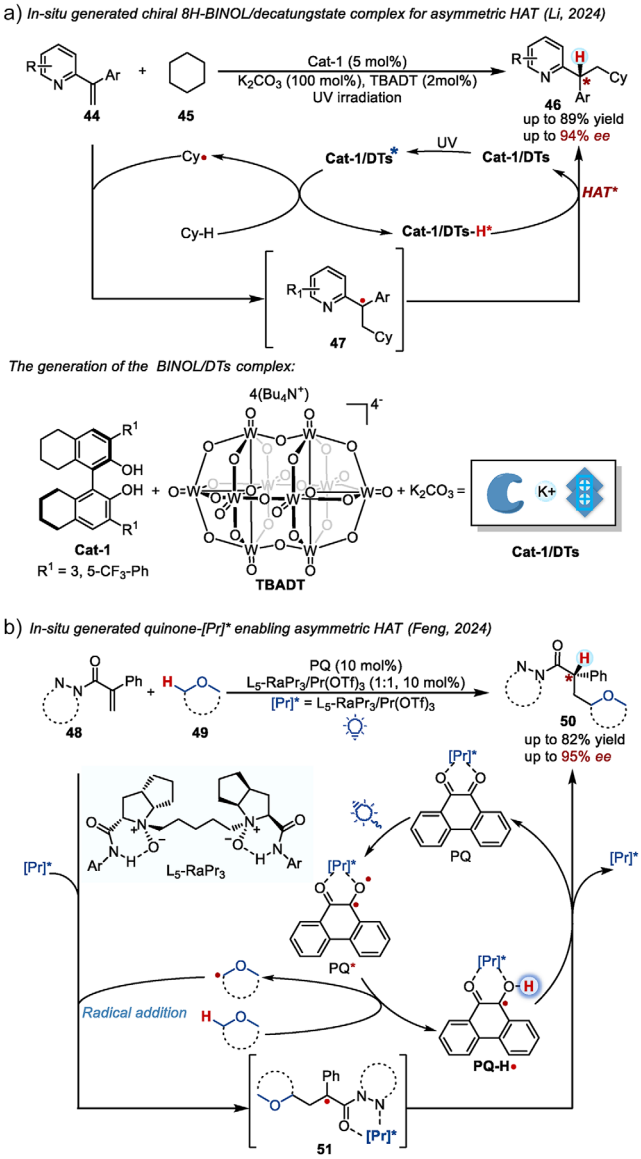

Scheme 7. In situ generation of chiral hydrogen donors for catalytic asymmetric HAT. a) In situ generated chiral 8H-BINOL/decatungstate complex for asymmetric HAT. b) In situ generated quinone-[Pr]* enabling asymmetric HAT.

chiral Lewis acid pocket orients the substrate and coordinates with the quinone photocatalyst, enabling an asymmetric HAT from the semiquinone radical (**PQ-H•**) to the prochiral radical intermediate. While yields and *ee* values varied with substrate class, this work demonstrated a novel strategy to merge photochemistry, Lewis acid templating, and chiral hydrogen-atom delivery.[49,50]

3. Radical-Centered Control

In donation-controlled HAT, stereochemistry is governed by the chiral environment of the hydrogen donor. By contrast, radical-centered control achieves enantioselection by pre-orienting and stabilizing the prochiral radical within a chiral

environment before hydrogen-atom delivery occurs. This approach decouples stereocontrol from the donor's intrinsic steric profile and instead leverages metal coordination, hydrogen bonding, or other noncovalent interactions to bias the trajectory of H-atom capture. As a result, it offers greater flexibility and often enables high selectivity.

3.1. Lewis-Acid Coordination

One of the most widely explored approaches to radical-centered control is the use of chiral Lewis acids to organize the radical intermediate in a defined chiral pocket. In pioneering work, Sibi developed a powerful platform for chiral Lewis acid-coordination induced enantioselective HAT reactions, enabling asymmetric hydrofunctionalization of electron-deficient olefins with anti-Markovnikov regioselectivity (Scheme 8a). In this radical-chain process, a tin radical generated from the radical initiation step abstracts a halogen atom from alkyl halide, producing an alkyl radical R•. This radical undergoes Michael addition to activated olefins **54** coordinated by a chiral Lewis acid, forming a prochiral carbon radical **55**, which is then reduced by tin hydride through an enantioselective HAT process, regenerating the tin radical to complete the chain process. By employing an indene-bisoxazoline $\mathbf{L_1}$*-Mg(II) complex as the chiral Lewis acid, various acrylates with distinct substituents, including protected amino groups, imide groups, and hydroxymethyl groups, were converted to the corresponding esters featuring α-chiral tertiary centers (eq 1- eq 3). This strategy yielded synthetically valuable motifs such as α-amino acid esters **58** (eq 1),[51] β-amino acids **60** (eq 2),[52] and β-hydroxy esters **62** (eq 3) in high enantioselectivities (Scheme 8b).[53] The rigid chelating complex formed between the radical and the chiral Lewis acid $\mathbf{L_1}$*-Mg(II) was proposed to adopt different ring sizes. Each of these complexes efficiently directed the approaching face of the ensuing HAT, resulting in excellent enantioselectivities.

The coordinating group in the radical was further extended to benzimidazolyl sulfonyl group by Toru's group (Scheme 8b). In the presence of a stoichiometric amount of $\mathbf{L_2}$*-Zn(II) (eq 4), the cascade radical addition and asymmetric HAT reaction afforded sulfone compounds **64** bearing α-chiral tertiary center with excellent efficiency and moderate to good enantioselectivities.[54] A tetrahedral zinc complex coordinated by sulfone and imidazole functionalities was proposed to rationalize the efficient enantiocontrol. Additionally, Sibi's group also extended this platform to substituted conjugate enones **65** (eq 5). In this case, the stereochemistry of the HAT process was controlled in a diastereoselective manner, influenced by both the rigid chelating of the Lewis-acid complex and the newly formed β-stereocenter in the radical addition step. It yielded both good enantioselectivities and excellent diastereoselectivities with the utilization of $\mathbf{L_3}$*-Al(III) Lewis acid.[55]

In this Lewis acid-coordination induction paradigm, stoichiometric or substoichiometric amounts of chiral Lewis acids are typically required to ensure high levels of enantiocontrol. Lower loadings significantly diminish enantioselectivity due

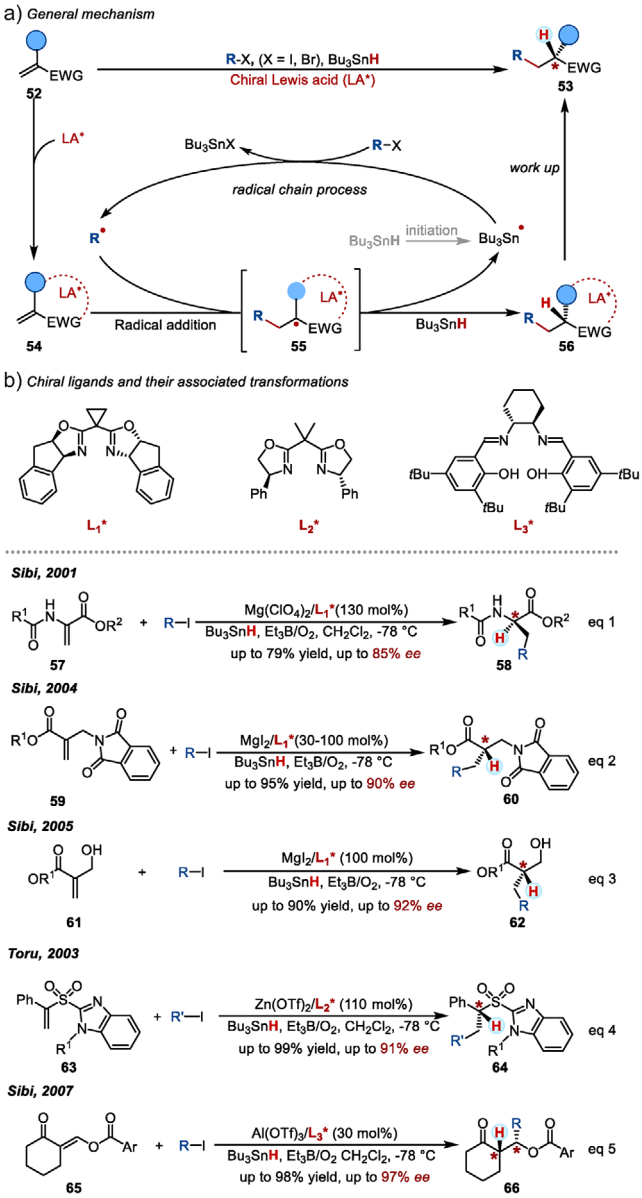

Scheme 8. Chiral Lewis acid–bound radicals enabling enantioselective HAT. a) General mechanism. b) Chiral ligands and their associated transformations.

to the presence of racemic background reactions involving uncoordinated substrates. To address the limitation of requiring high amounts of Lewis acids, an effective solution could be cooperative integration of the prochiral carbon radical generation and its termination with a shared metal complex, thereby reducing the necessary amount of chiral Lewis acid while maintaining high levels of enantiocontrol.

3.2. Metal-Redox Integrating Radical Generation with Chiral Termination

A particularly attractive branch of radical-centered control is to integrate radical generation and enantioselective

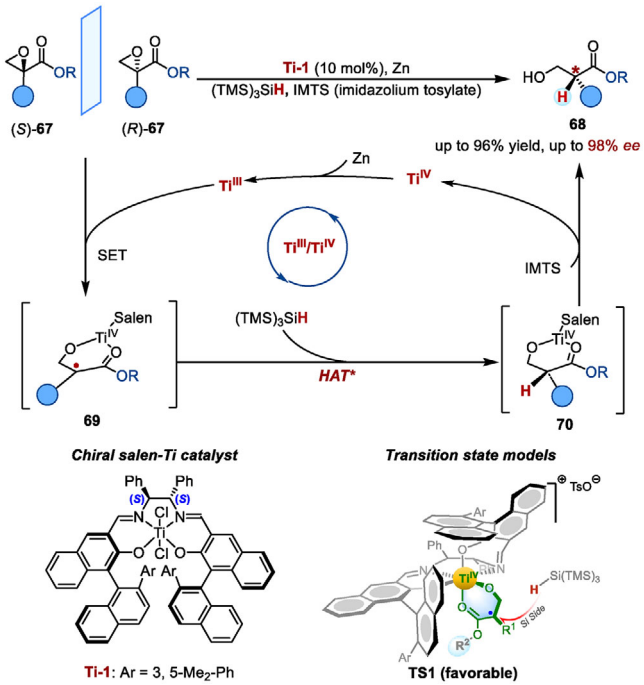

Scheme 9. Ti(III)/Ti(IV) redox catalysis enabling asymmetric HAT through integrated radical generation and enantioselective termination (Zhang, 2022).

termination within a single chiral metal complex, creating a tightly coupled catalytic cycle that reduces the need for stoichiometric Lewis acids and suppresses racemic background pathways. An early and influential demonstration of this idea came from Gansäuer and co-workers, who used Ti(III)/Ti(IV) redox chemistry to generate substrate-bound radicals and channel them through intramolecular HAT events with high diastereoselectivity. Although this work did not achieve true enantioselective HAT—stereocontrol arose from the substrate's own conformational bias—it established the feasibility of metal-coordinated radical confinement and inspired later developments in fully enantiocontrol systems.[56,57]

Building on this foundation, Zhang and co-workers introduced a Ti(III)/Ti(IV) metal redox strategy that allows integration of both radical generation and termination through HAT, facilitating catalytic asymmetric HAT reactions within the coordination-induction framework (Scheme 9). The mechanism exploits the single-electron redox properties of Ti(III)/Ti(IV), where (Salen)Ti(III) facilitates the homolytic cleavage of the C─O bond in the epoxide through SET, generating a chelated radical intermediate **69**. This radical undergoes an enantioselective HAT step, with (Salen)Ti(IV) acting as a chiral Lewis acid to discriminate the approach of $(TMS)_3SiH$ to the radical center. The enantioconvergent mechanism relies on successive stereoablation of epoxide **67** and enantioselective HAT processes. Detailed experiments revealed a modest kinetic resolution with (Salen)Ti(III) in the ring-opening stage ($k_R/k_S = 2.3$) and excellent enantiocontrol by (Salen)Ti(IV) in the HAT step, achieving both high efficiency and stereoselectivity within a reasonable reaction time. This redox strategy enabled the enantioselective transformation of racemic glycidic esters and amides into formal formaldehyde aldol adducts **68**.[58]

This metal–redox strategy represents a Lewis acid-coordination paradigm shift: within a single catalytic cycle, the reduced metal center promotes radical generation, while the oxidized metal center functions as a chiral Lewis acid to coordinate and orient the radical, enforcing enantioselective HAT. In this way, radical generation and stereocontrolled termination are seamlessly integrated into one unified redox-driven process.

3.3. Noncovalent Templates and H-Bonding

Beyond metal coordination, noncovalent interactions—especially hydrogen bonding—provide a complementary strategy for stereocontrol in asymmetric HAT. By positioning the radical intermediate in a preorganized chiral environment, these systems enable facial differentiation without relying on strong Lewis acid binding and are therefore broadly compatible with sensitive substrates. In particular, the Bach group has developed a series of hydrogen-bond-donor catalysts that utilize carefully arranged hydrogen-bonding networks to achieve precise stereocontrol in radical processes (Scheme 10a).

A landmark example was reported in 2004 by Bach and co-workers, who achieved an intramolecular radical addition to α,β-unsaturated lactams followed by an enantioselective HAT step (Scheme 10b).[59] In this system, the rigid bicyclic amide template **HBT-1** functions as a hydrogen-bonding framework that both donates and accepts hydrogen bonds, thereby locking the radical intermediate **73**—formed through sequential halogen abstraction from substrate **71** by a tin radical and radical cyclization—into a well-defined geometry. The bulky tetrahydronaphthalene moiety sterically shields the *Re* face of the radical, guiding H-atom delivery preferentially from the *Si* face. This radical chain cyclization of **71** proceeded in high yield and with impressive enantioselectivity, establishing hydrogen-bond templating as a viable strategy for catalytic asymmetric HAT.

Building on this concept, Bach later developed a photoinduced radical deracemization strategy for hydantoins (Scheme 10c).[60] The chiral benzophenone catalyst **HBT-2** forms a hydrogen-bonded complex selectively with one substrate (*S*)-**74**. Upon light excitation, the carbonyl group of **HBT-2** abstracts a hydrogen atom from the stereogenic center (C5) of the (*S*)-**74** to generate radical intermediate **76**. This radical pair undergoes reversible HAT, which, after dissociation and recombination, can return either enantiomer of the (*R*)-**74**. Because catalyst **HBT-2** preferentially binds and activates (*S*)-**74**, this enantiomer is continuously recycled through the HAT cycle, while the opposite enantiomer (*R*)-**74** accumulates over multiple turnovers, leading to significant enantiomeric enrichment. Owing to its mild, reversible noncovalent interactions, this strategy is tolerant of diverse functional groups and avoids issues with metal residues, making it an attractive complement to Lewis acid–based approaches.

The strategy was also successfully extended to the photochemical deracemization of 3-substituted oxindoles **78**[61]

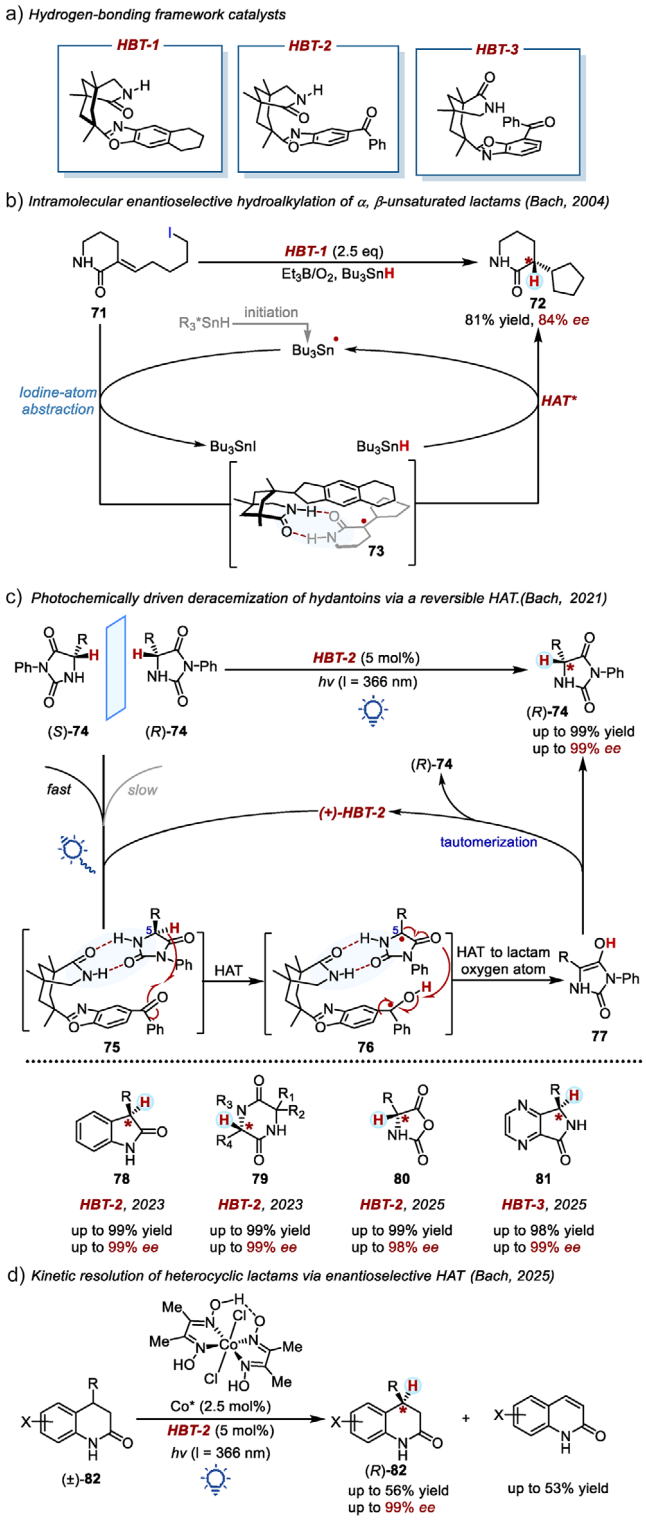

Scheme 10. Hydrogen-bond templating strategies for asymmetric HAT. a) Hydrogen-bonding framework catalysts. b) Intramolecular enantioselective hydroalkylation of α,β-unsaturated lactams. c) Photochemically driven deracemization of hydantoins via a reversible HAT. d) Kinetic resolution of heterocyclic lactams via enantioselective HAT.

and 2,5-diketopiperazines **79**,[62] utilizing the enantiomer of **HBT-2**. Transient absorption spectroscopy confirmed the selective HAT mechanism. The catalyst's triplet state exhibited a longer lifetime (550 ns) with the matched substrate (*R*)-**79**, forming a persistent protonated ketyl radical (>1 ms). Recently, the same research group achieved the photochemical deracemization of N–carboxyanhydrides through a reversible HAT process using **HBT-2** as hydrogen-bonding donor, enabling the synthesis of chiral α–amino acid derivatives **80** with high *ee*.[63]

Guided by molecular model analysis and preliminary calculations, the authors repositioned the photoactive benzoyl group in **HBT-2** from the 5– to the 7–position on the benzoxazole scaffold. This structural modification led to the next–generation catalyst **HBT-3**, which was specifically optimized for the photochemical deracemization of 3–substituted 4,7–diaza–1–isoindolinones **81**. DFT calculations and H/D crossover experiments indicate that only (*S*)-**81** is processed by the **HBT-3**, while (*R*)-**81** remains unreactive. The computations reveal that the back-HAT preferentially occurs at the N4 position, generating an enamine intermediate, which likely contributes to the higher catalytic efficiency as reflected in the significantly reduced catalyst loading of 2.5 mol%.[64]

More recently, a synergistic system combining photocatalysis with cobaloxime-mediated dehydrogenation has been developed for the kinetic resolution of lactams (±)-**82** (Scheme 10d).[65] In this system, the catalyst **HBT-2** selectively mediates HAT from (*S*)-**82**. Therein, an irreversible cobalt-catalyzed oxidation enables the recovery of the unreacted (*R*)-**82** in high enantiopurity with excellent *s* factors.

4. Abstraction-Controlled HAT

While donation- and radical-centered HAT strategies rely on controlling radical termination after hydrogen-atom capture, an alternative is to introduce stereocontrol at the very moment the C–H bond is cleaved. In such a hydrogen-atom abstraction (HAA), a chiral hydrogen abstractor selectively removes a hydrogen atom from one enantiotopic site of a prochiral substrate or reacts at different rates with each enantiomer of a racemic mixture. The resulting carbon-centered radical can then be trapped in a stereoretentive fashion—preserving the configuration installed during abstraction—or intercepted nonselectively. This mechanistic mode of control is conceptually distinct from donation- or radical-centered HAT, since enantioselection coincides directly with C–H activation. The reported examples can be grouped into kinetic resolutions and desymmetrization.

4.1. Kinetic Resolution via HAA

Early proof-of-principle for HAA-enabled kinetic resolution came from Roberts in 1991,[66] who introduced the first catalytic enantioselective HAA with PRC strategy (Scheme 11). Photolysis of di-tert-butyl peroxide generated *t*BuO•, which

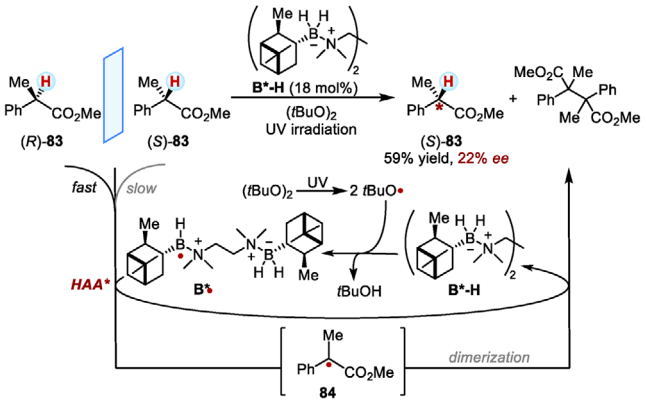

Scheme 11. Catalytic asymmetric HAA using PRC strategy (Roberts, 1991).

abstracted hydrogen from a chiral amine–borane **B*-H**, generating a nucleophilic boryl radical **B***•. This species then performed enantioselective HAA at the α-position of racemic ester **83**, regenerating the chiral catalyst and giving α-carbonyl radical **84** that dimerized or coupled further. As a consequence, the starting ester was converted to enantioenriched (*S*)-**83** through a kinetic-resolution pathway, albeit with only modest selectivity (59% yield, 22% *ee*). Although enantioselectivity was limited, this work provided the first clear model for asymmetric HAA and demonstrated the feasibility of catalyst-controlled C─H abstraction. Subsequent studies employed ESR spectroscopy to directly measure enantioselectivity,[67] expanded the scope to ketones with a steric-strain model,[68] elucidated the mechanistic origins via X-ray and computation,[69] and finally extended the strategy to silicon-centered radicals for Si─H abstraction.[70] This series of work established a robust and evolving platform for catalyst-controlled enantioselective functionalization of C─H and Si─H bonds.

Liu and co-workers later demonstrated that a chiral Mn–salen catalyst, oxidized in situ to Mn(V) = O (Scheme 12), enantioselectively abstracts hydrogen-atom from tertiary propargylic C─H bonds in **85**. The resulting radicals **87** undergo stereoretentive oxygen rebound with Mn(IV)─OH, furnishing enantioenriched alcohols **86** and recovering the remaining starting material (*S*)-**85** in high enantiopurity.[71] This work shows how metal–oxo species can combine enzymatic-like recognition with radical reactivity in a kinetic resolution process. The same group also applied this kinetic resolution strategy for the transformation of saturated ethers and benzylic azides.[72–74]

An elegant complementary strategy was reported by Einhorn and colleagues, who designed axially chiral N-hydroxyimide catalysts that generate C_2-symmetric nitroxyl radicals (Scheme 13).[75,76] These radicals perform enantioselective HAA on racemic N-acyl oxazolidines **88**, after which the radicals **90** are trapped by O_2 to effect oxidative ring-opening, furnishing **89**. Fine-tuning of the catalyst scaffold yielded exceptional selectivity factors ($s > 50$), establishing a highly efficient radical-based kinetic resolution platform via asymmetric HAA.

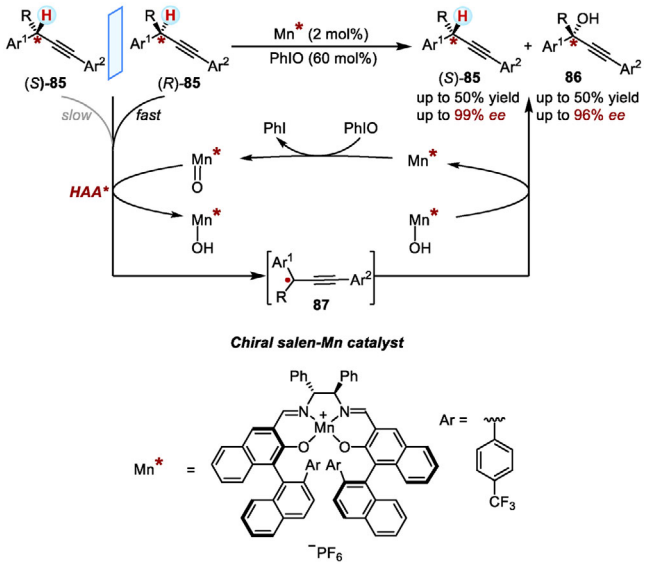

Scheme 12. Kinetic resolution of tertiary propargylic substrates by chiral Mn–salen mediated HAA (Liu, 2024).

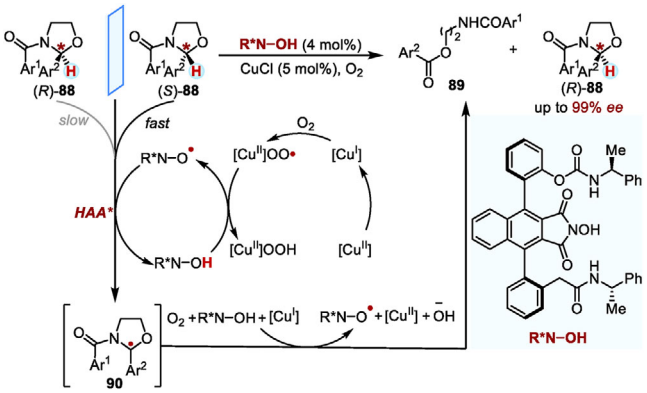

Scheme 13. Axially chiral N-hydroxyimide catalysts for enantioselective HAA leading to kinetic resolution of N-acyl oxazolidines (Einhorn, 2007).

4.2. Desymmetrization via HAA

Parallel to kinetic resolution, organocatalytic strategies have expanded the power of HAA for desymmetrization. Phipps reported that Cinchona alkaloid–derived amines **94**, upon photooxidation, generate aminium radical cations **95** that enantioselectively abstract hydrogen atom from meso-diols **91** (Scheme 14a). Mechanistic studies indicate that the key HAA step was confirmed as both rate- and enantio-determining, and the resulting radicals **93** were reduced by thiol donors via a diastereoselective HAT to deliver chiral trans-diols **92** with excellent enantioselectivity.[77]

Building upon this foundation of enantioselective diol desymmetrization via HAA, the same research group subsequently introduced a complementary photocatalytic oxidative strategy. In this oxidative variant, oxidatively quenched 4CzIPN generates a quinuclidinium radical cation **100** that abstracts hydrogen from the same class of meso-diols **96** (Scheme 14b).[78] Rather than being reduced, the resulting

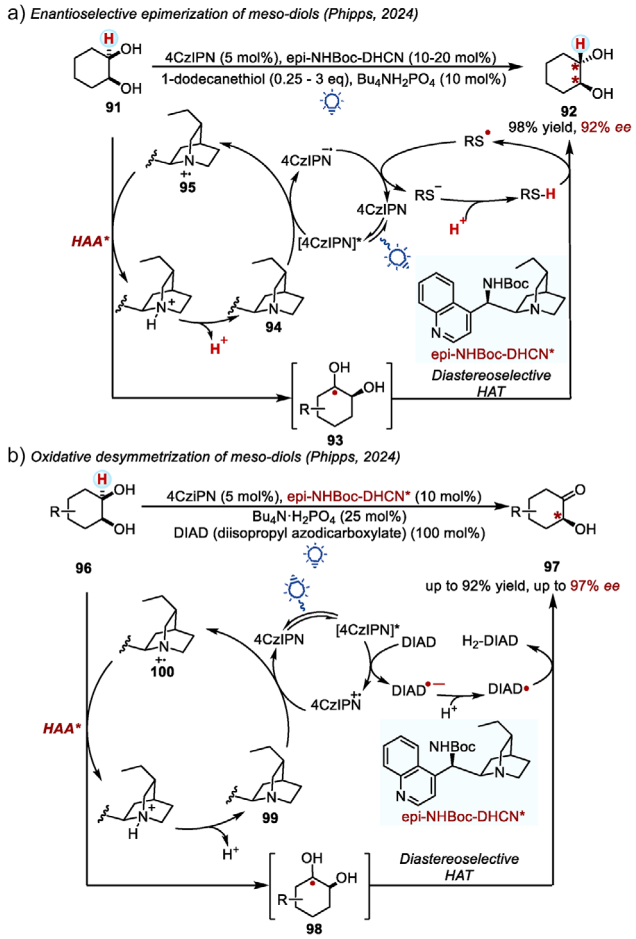

Scheme 14. Quinuclidine-based organocatalytic enantioselective HAA for desymmetrization of meso-diols. a) Enantioselective epimerization of meso-diols. b) Oxidative desymmetrization of meso-diols.

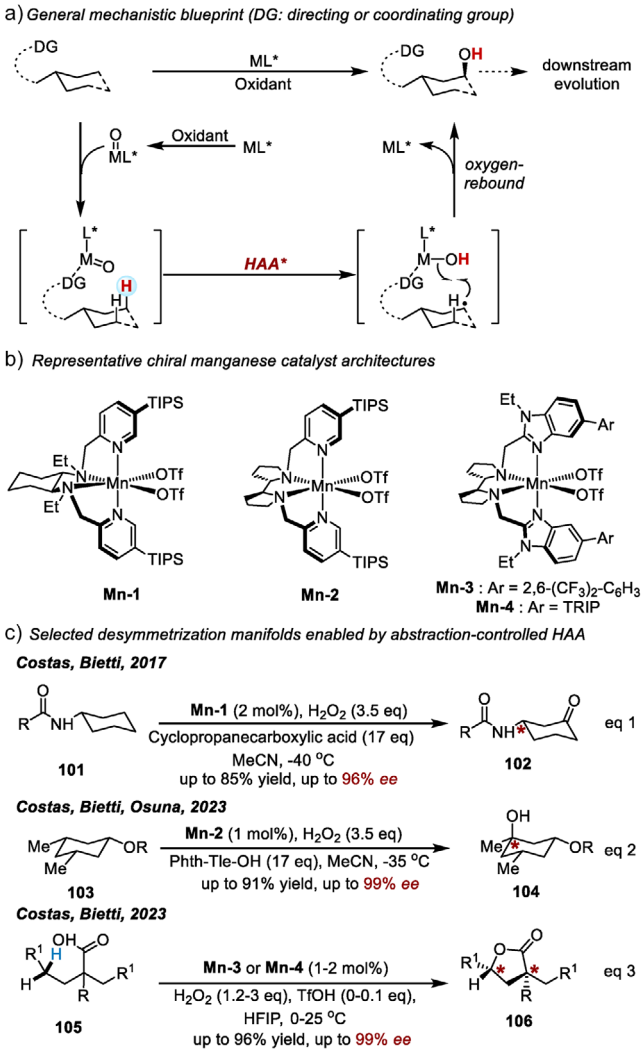

Scheme 15. Abstraction-controlled desymmetrization via chiral metal–oxo HAT. a) General mechanistic blueprint. b) Representative chiral manganese catalyst architectures. c) Selected desymmetrization manifolds enabled by abstraction-controlled HAA.

ketyl radicals **98** are intercepted by DIAD•$^-$ or O_2, delivering α-hydroxyketones **97** in up to 97% *ee*. Notably, this approach is broadly applicable to cyclic and acyclic diols and even allows multiple stereocenters to be established in a single operation.

A distinct manifestation of abstraction-controlled asymmetric HAT is found in the desymmetrization of meso and prochiral substrates by high-valent metal–oxo species. In these systems, a chiral M═O unit engages a substrate bearing enantiotopic C─H bonds and enforces stereodifferentiation at the hydrogen-atom abstraction stage (Scheme 15a). The ensuing carbon-centered radical retains configurational bias and undergoes rapid oxygen rebound to form a C─O bond, thereby translating HAA selectivity into stable molecular chirality. Depending on substrate topology, the nascent alcohol may be further oxidized or participate in intramolecular cyclization, enabling direct access to complex chiral scaffolds.

Katsuki and co-workers provided an early demonstration of this concept through Mn–salen-catalyzed enantiotopic C─H oxidation of meso-tetrahydrofurans, delivering optically active lactols via desymmetrizing HAA.[79] Mechanistic analysis revealed that enantioselection originates from differential hydrogen abstraction from enantiotopic C─H bonds, rather than from the rebound step itself.

Building on this paradigm, Costas, Bietti, and Osuna developed a family of sterically encumbered manganese catalysts that enable enantioselective oxidation of non-activated aliphatic C─H bonds (Scheme 15b). A chiral Mn═O species selectively abstracts one of two enantiotopic C─H bonds within a hydrocarbon framework, generating a configurationally biased carbon radical that undergoes rapid oxygen rebound. Depending on substrate class and reaction design, this abstraction-controlled event can be translated into multiple desymmetrization manifolds (Scheme 15c): tertiary C─H hydroxylation of cyclohexane derivatives **101** is followed by in situ overoxidation, furnishing chiral cyclohexanones **102** bearing a stereogenic β-carbon center (eq 1);[80] direct realization, selective HAA/rebound yields enantioenriched tertiary alcohols **104**, allowing simple hydrocarbons to be converted into chiral alcohols in a single step (eq 2);[81] and substrates equipped with a carboxylic acid tether **105** undergo intramolecular capture of the nascent radical, enabling highly

enantioselective γ-lactonization of non-activated C─H bonds (eq 3).[82] Across these transformations, enantioselection is set at the HAA stage through substrate recognition within a sterically and electronically sculpted chiral pocket, while subsequent rebound or oxidation steps are rapid and largely stereoretentive.

A mechanistically distinct but conceptually related desymmetrization strategy was pioneered by Zhang and co-workers using cobalt radical catalysis (Scheme 16a). In these systems, sulfamoyl azides **107** are activated by Co(II)–HuPhyrin complexes to generate α-Co(III)-aminyl radicals **109**, which undergo enantioselective intramolecular HAA as the key stereodetermining step. The radical **110** then undergoes stereoretentive C─N bond formation, as the confined chiral cavity prevents racemization by restricting rotation around the α-C bond, a conclusion supported by KIE studies and DFT calculations. Careful ligand engineering enabled excellent enantioselectivities and even enantiodivergence by altering non-chiral elements of the HuPhyrin framework. This represents a powerful extension of desymmetrization by HAA into asymmetric C─H amination, showcasing the versatility of radical intermediates confined in a metalloradical pocket.[83]

The same group further reported that alkoxysulfonyl azides **111** derived from simple alcohols (Scheme 16b),[84] serve as effective substrates for the synthesis of β-functionalized chiral amines **112**. This work rigorously dissected the stereodetermining step: KIE studies with enantiopure, deuterium-labeled substrates quantitatively established the enantioselectivity of the HAA step. Specifically, the intramolecular KIEs measured with chiral catalyst [Co(Por*)] were found to be highly divergent for the two enantiomers ($KIE_{(S)\text{-}\mathbf{111_D}} = 0.2$, $KIE_{(R)\text{-}\mathbf{111_D}} = 44$). When the same chiral catalyst was employed, it was observed that the experimental enantiomeric excess of the product was significantly higher than the calculated value based solely on the facial selectivity established in the HAA step, for both (*S*)-$\mathbf{111_D}$ and (*R*)-$\mathbf{111_D}$. Together, these quantitative discrepancy clearly confirms that the subsequent radical substitution step proceeds in a stereoretentive manner and contributes cooperatively to the overall enantioselectivity. These experiments validate that steps of both HAA and radical substitution cooperatively controlled the enantioselectivity of the Co(II)-catalysed 1,5-C-H amination.

More recently, Zhang and colleagues extended the strategy to a Fe(III)-based system for the asymmetric intramolecular C─H amination of aryl azides **113**, enabling efficient access to chiral indolines **114**. DFT calculations indicated that the 1,5-HAA step serves as the enantiodetermining event in the reaction (Scheme 16c).[85]

Together, these studies establish HAA as a conceptually straightforward yet increasingly versatile approach to enantiocontrolled radical chemistry.[86] In both kinetic resolution and desymmetrization, the decisive event is the selective C─H cleavage itself, while subsequent radical capture—when stereoretentive—preserves the chiral information introduced at that instant. This conceptual clarity, now paired with organocatalytic and metalloradical designs, ensures that abstraction-controlled HAT will remain a fertile and expanding strategy for asymmetric radical chemistry.

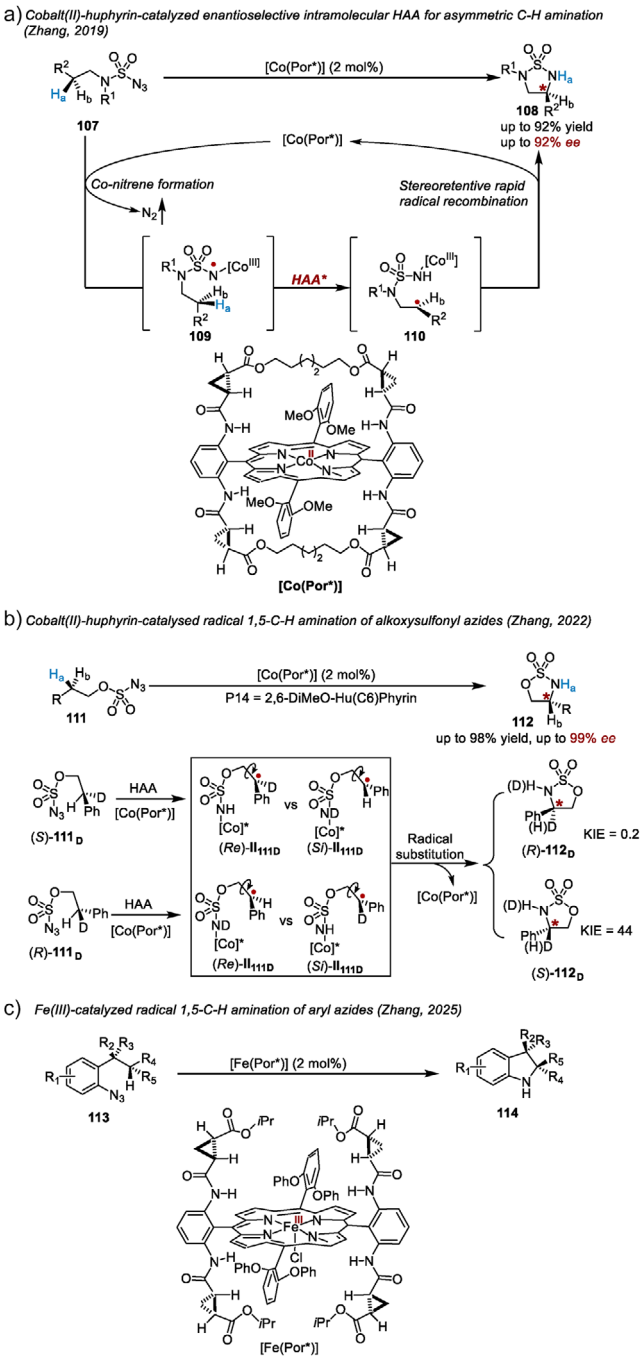

Scheme 16. Aa) Cobalt(II)-Huphyrin-catalyzed enantioselective intramolecular HAA for asymmetric C─H amination. b) Cobalt(II)-Huphyrin-catalysed radical 1,5-C-H amination of alkoxysulfonyl azides. c) Fe(III)-catalyzed radical 1,5-C-H amination of aryl azides.

5. Cooperative Bimetallic Catalytic Platforms

The strategies discussed above achieve stereocontrol by isolating a single enantiodetermining event—whether hydrogen donation, radical templation, or hydrogen abstraction. A complementary paradigm is to merge these steps into a single, highly organized catalytic manifold in which both

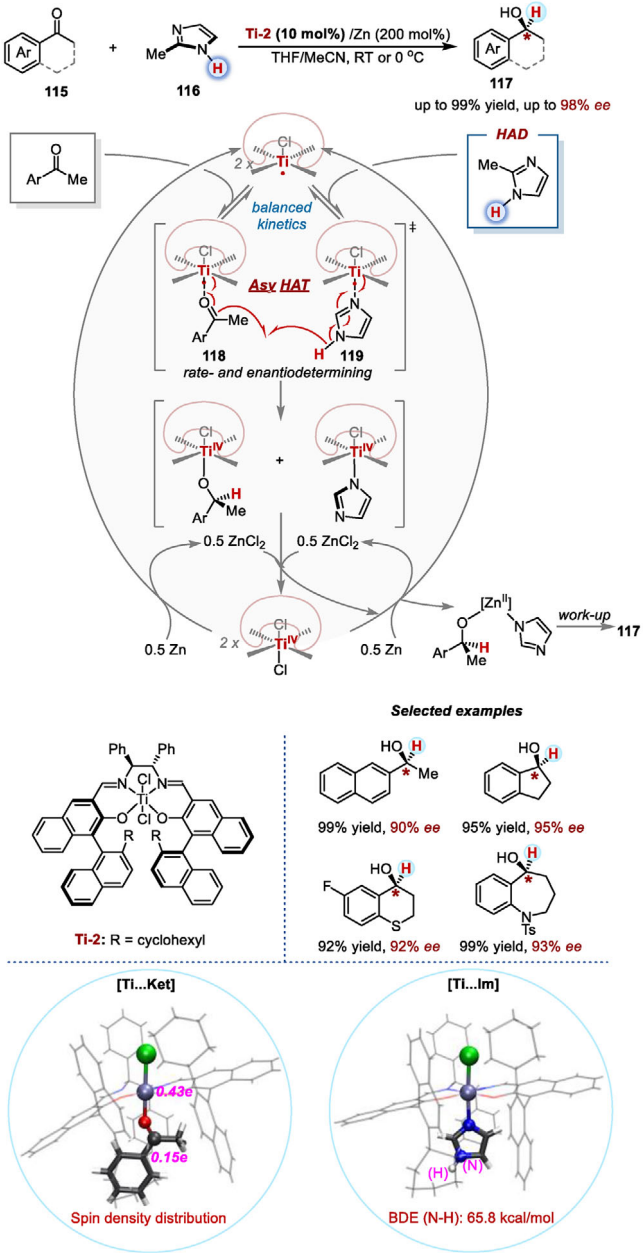

Scheme 17. Cooperative bimetallic (salen)Ti catalysis for concerted asymmetric HAT (Zhang, 2025).

the hydrogen-atom donor and acceptor are simultaneously activated within a chiral environment. In this cooperative mode, HAT proceeds in a concerted fashion without the accumulation of free carbon-centered radicals, thus minimizing racemic background and expanding the accessible range of hydrogen donors and acceptors. Such systems offer a conceptual departure from stepwise radical control and open opportunities for sustainable asymmetric HAT.

A landmark example of this concept was recently reported by Zhang's group (Scheme 17).[87] They developed a cooperative bimetallic radical catalysis using two chiral (salen)titanium complexes that independently engage the hydrogen donor imidazole **116** and the hydrogen acceptor aryl ketone **115**, orchestrating a concerted, stereocontrolled HAT from N─H to C═O functionality. In this system, one Ti(III) complex binds and polarizes the imidazole N─H bond (**119**), lowering its BDE and enabling homolytic cleavage, while a second Ti(III) complex activates the ketone acceptor (**118**) through single-electron reduction. The key HAT event then occurs within a preorganized bimetallic chiral pocket, which leads to an excellent enantioselectivity. Crucially, this strategy avoids free ketyl radicals formation that may lead to background racemic or side reactions.

Mechanistic studies support a dual activation and concerted HAT pathway. Kinetic analysis showed strict second-order dependence on the titanium catalyst and a positive nonlinear effect, indicating cooperative involvement of two chiral (salen)Ti complexes in the stereodetermining step. Control experiments confirmed the titanium–imidazole complex as the true H-donor: conventional donors such as Bu_3SnH or H-blocked N-methylimidazole were ineffective. A moderate KIE (2.4) with N─D imidazole suggests N─H cleavage is rate-limiting, while radical-probe experiments revealed only minimal contribution from free-radical pathways. Complementary DFT calculations revealed a substantial weakening of the imidazole N─H bond upon Ti coordination in **[Ti…Im]**, and Ti-centered spin density in the complex of **[Ti…Ket]**, consistent with a metal-bound, concerted hydrogen transfer event.

This cooperative bimetallic platform exhibits broad substrate scope and synthetic utility. A wide range of aryl, heteroaryl, and benzo-fused cyclic ketones were reduced with up to 98% *ee*, including pharmaceutically relevant scaffolds, such as intermediates for tolvaptan. Catalyst loading can be reduced to 5 mol% with minimal erosion of performance, demonstrating scalability and practical potential.

Mechanistically and conceptually, this mode is distinct from prior asymmetric HAT approaches: by preorganizing both donor and acceptor in a bimetallic chiral pocket and bypassing free carbon radicals, it suppresses racemic background, accommodates stronger N─H donors such as imidazole, and creates new space for designing stereocontrolled HAT with unconventional donors.

6. Biocatalytic Platforms for Asymmetric HAT

Enzymes offer a uniquely elegant solution to the long-standing challenges of asymmetric HAT. Within an enzymatic active site, radical generation, chiral preorganization, and hydrogen delivery are co-localized and orchestrated with exquisite spatial and temporal control.[88,89] In this way, enzymes function as built-in synergistic platforms, effectively integrating these mechanistic elements. Therein, the radicals are produced under mild redox or photoredox conditions, held in a highly defined chiral pocket through precise enzyme–substrate interactions, and then terminated by a stereoselective HAT step mediated by a cofactor. This confinement suppresses racemic background pathways and

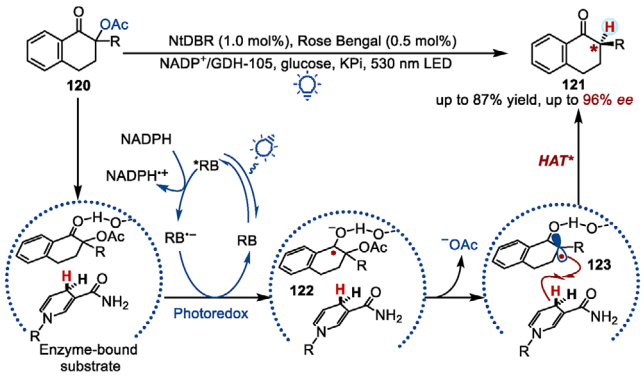

Scheme 18. Photoredox–ERED cooperative catalysis for enantioselective HAT with NADPH (Hyster, 2018).

routinely delivers exceptional levels of enantioselectivity under environmentally benign conditions.

Notably, enzymatic HAT is almost always coupled to naturally evolved hydrogen carriers — most prominently NADPH and FMN. These cofactors not only supply the reactive hydrogen-atom but also participate in subtle conformational gating and electronic tuning within the enzyme active site, helping to enforce precise facial selectivity during radical quenching. On this basis, we classify emerging biocatalytic HAT systems by the identity of the hydrogen donor cofactor, treating the mode of radical generation (e.g., photoredox, reductive activation) as a secondary dimension. This donor-centered framework provides a unifying perspective for otherwise diverse enzymatic HAT platforms.[90–93] Given the rapid growth of biocatalytic asymmetric HAT, we limit our following discussion to representative examples that showcase its key mechanistic advances.

6.1. NADPH-Donor Manifolds

In these enzymatic platforms, reduced NADPH functions as the hydrogen-atom donor, and enantioselection is set when the radical intermediate receives H• from the nicotinamide ring, precisely oriented within the chiral enzyme pocket.

6.1.1. Photoredox–Enzyme Cooperative Catalysis

Hyster and co-workers pioneered the merger of visible-light photoredox catalysis with NADPH-dependent double-bond reductases to achieve asymmetric radical reductions under mild conditions (Scheme 18).[94] In this system, the external photocatalyst Rose Bengal promotes single-electron reduction and decarboxylation of α-acetoxyketones **120** to generate α-carbonyl radical **123**. The radical enters the enzyme's active site, where substrate binding lowers the reduction potential and enforces a rigid, chiral orientation. Within this well-defined pocket, NADPH delivers the hydrogen-atom enantioselectively, converting the radical **123** into an α-stereogenic ketone **121** in up to 96% *ee*.

6.1.2. Photoexcited Ketoreductases (KREDs)

Beyond photoredox–enzyme cooperativity, the NADPH cofactor plays a dual role: it serves as the electron donor to reduce the substrate and, in its ensuing oxidized form, as the enantioselective hydrogen-atom source within the ketoreductase (KRED) active site. In these systems, the enzyme forms an EDA complex with its bound substrate; direct visible-light excitation triggers SET from NADPH to the substrate, generating a carbon-centered radical within the chiral active site. This radical is then terminated by enantioselective HAT from NADPH•$^+$, allowing asymmetric C–H bond formation without an external photocatalyst. Such direct photoexcitation expands the biocatalytic toolbox and simplifies reaction design by merging radical initiation and stereocontrolled hydrogenation in one protein pocket. Several landmark demonstrations illustrate the versatility of this concept:

Reductive Dehalogenation of α-Bromolactone. In a pioneering study, Hyster's group showed that α-bromolactones **124** bound to KRED form an EDA complex **126** that absorbs visible light (Scheme 19a). SET from NADPH produces a lactonyl radical **127** and NADPH•$^+$. Following HAT from NADPH•$^+$ to the prochiral radical, the reduction product **125** is generated, and the cofactor is oxidized to NADP$^+$, which is then reduced to NADPH by either isopropyl alcohol (using native alcohol dehydrogenase activity) or glucose dehydrogenase.[95]

Decarboxylative Hydroalkylation of Alkenes. Zhao and co-workers extended the platform to N-(acyloxy)phthalimides (Scheme 19b), where light-driven EDA excitation inside KRED triggers N–O bond cleavage of **128** and decarboxylation to form a benzylic radical **132**. This radical adds to alkenes **129**, and subsequent NADPH-mediated HAT delivers α-stereogenic carbonyl products **130** with excellent enantioselectivities.[96]

Hydroalkylation of Enamines. Huang and Wang employed imine reductases (IREDs) for photoenzymatic radical hydroalkylation (Scheme 19c). Visible-light excitation of an EDA complex **137** between IRED-bound NADPH and a pyridinium radical precursor **134** generates an alkyl radical **138**, which adds to enamides **135**. The resulting prochiral α-amido radical **139** undergoes stereocontrolled HAT from NADPH•$^+$ within the enzyme's active site, delivering chiral amines with high enantioselectivity. This work enables a challenging remote C(sp^3)–C(sp^3) bond formation via direct photoactivation of IREDs.[97]

6.2. FMN-Donor Manifolds

FMN cofactors embedded in ene-reductases (EREDs) offer a distinct strategy for asymmetric HAT. In these enzymes, the reduced or semiquinone form of FMN (FMN_{hq}/FMN_{sq}) serves both as a single-electron donor and as the stereocontrolled hydrogen source. After substrate activation by SET, the newly formed radical remains confined in the chiral pocket and is quenched by facially selective H-atom delivery from the N_5 position of the isoalloxazine ring, setting the stereocenter within a single, well-organized active site.

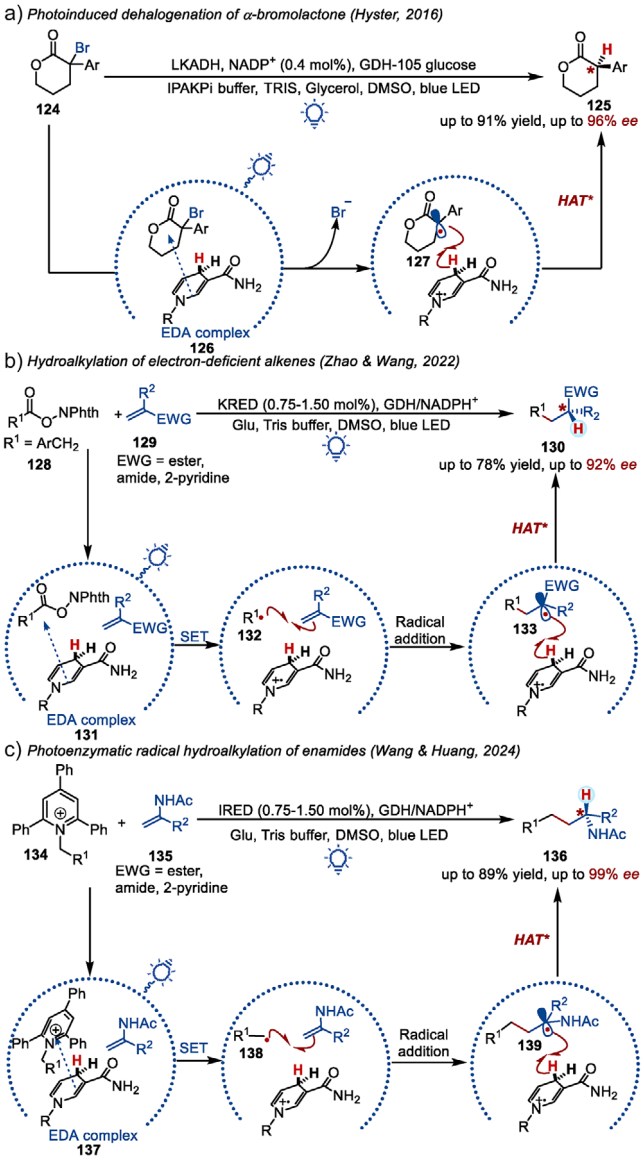

Scheme 19. Direct photoexcitation of ketoreductases (KREDs) enables NADPH-driven enantioselective HAT. a) Photoinduced dehalogenation of α-bromolactone. b) Hydroalkylation of electron-deficient alkenes. c) Photoenzymatic radical hydroalkylation of enamides.

6.2.1. Dark Flavin Cycles

In contrast to photoinitiated systems, "dark" flavin catalysis exploits the native redox activity of the reduced flavin cofactor (FMN_{hq}) under thermal conditions. FMN_{hq} delivers a single electron to electrophilic substrates such as α-bromoesters, inducing mesolytic C–Br cleavage and generating a radical intermediate confined within the enzyme active site. The resulting radical is then intercepted by facially selective HAT from the semiquinone form FMN_{sq}, establishing the stereocenter with high fidelity. Hyster and co-workers provided a landmark demonstration of this mode of reactivity: wild-type ene-reductases (EREDs) catalyze the reductive dehalogenation of α-bromoesters **140** without any external photocatalyst, furnishing α-chiral esters **141** in

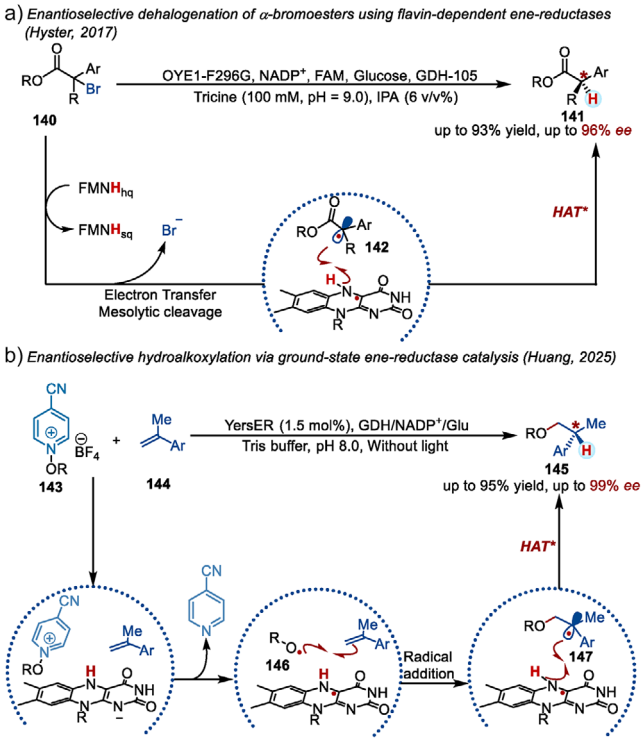

Scheme 20. Dark flavin catalysis: ERED-mediated reductive dehalogenation via enantioselective HAT. a) Enantioselective dehalogenation of α-bromoester using flavin-dependent ene-reductases. b) Enantioselective hydroalkoxylation via ground-state ene-reductase catalysis.

up to 96% *ee* (Scheme 20a).[98] This study revealed that EREDs can autonomously mediate both radical generation and stereocontrolled H-atom delivery, inaugurating the field of thermal ("dark") radical biocatalysis.

In 2025, Huang and co-workers accomplished the enantioselective intermolecular hydroalkoxylation of alkenes via a light-independent (Scheme 20b), ground-state SET mechanism. The strategy bypasses photoexcitation by utilizing reduced flavin (FMN_{hq}) to generate alkoxy radicals **146** from N-alkoxypyridinium salts **143**. Crucially, the HAT step from FMN_{sq} to the prochiral benzylic radical **147** was identified as the stereodetermining step. QM/MM calculations and KIE experiments confirmed that the enantiodiscrimination originates from differential HAT barriers within the enzyme's chiral pocket, enabling high enantioselectivity.[99] In the same year, Xu's group achieved stereoselective hydrotrifluoromethylation without light irradiation by employing trifluoromethyl thianthrenium triflate ($TT\text{-}CF_3{}^+OTf^-$) as the radical precursor.[100]

6.2.2. Photoredox–Flavin Catalysis

Building on the intrinsic redox and hydrogen-donating ability of flavin cofactors, researchers have paired visible-light photoredox catalysis with FMN-dependent ene-reductases (EREDs) to unlock radical transformations beyond native metabolism. In these systems, an external photocatalyst

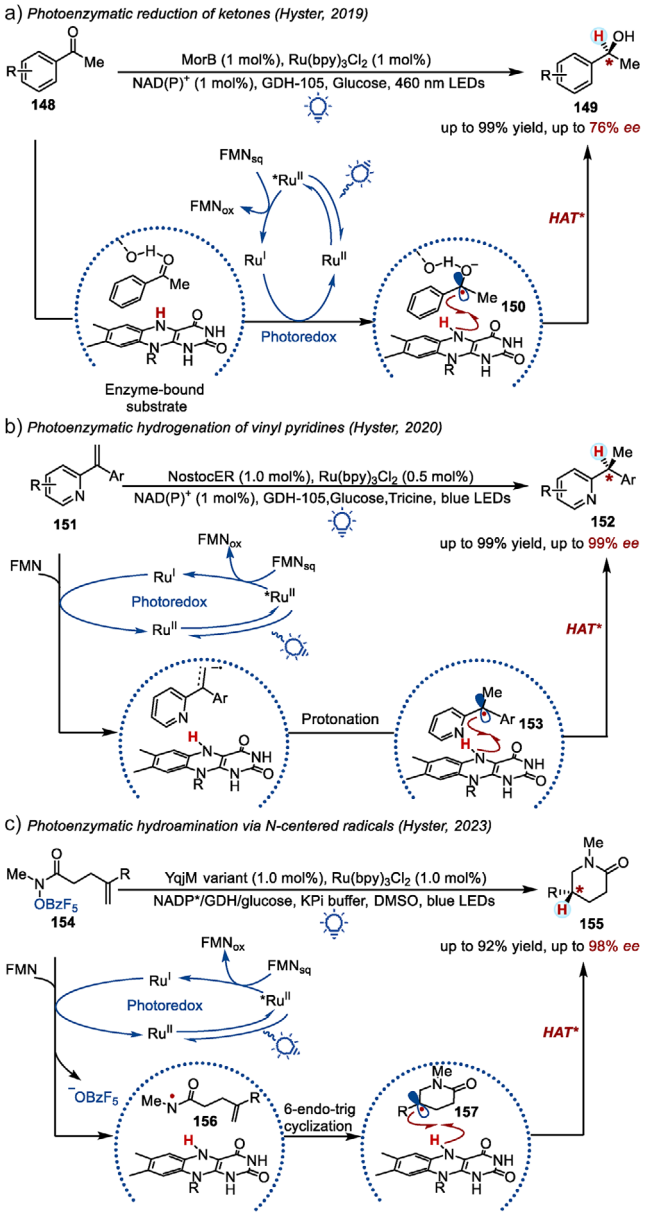

Scheme 21. Photoredox–ERED cooperativity: visible-light radical generation coupled with FMN-guided enantioselective HAT. a) Photoenzymatic reduction of ketones. b) Photoenzymatic hydrogenation of vinyl pyridines. c) Photoenzymatic hydroamination via N-centered radicals.

initiates radical formation under mild conditions, while the enzyme active site binds and preorganizes the substrate. The flavin cofactor—typically FMN—then serves as the stereocontrolled hydrogen-atom donor, forging products with high enantioselectivity. Several landmark demonstrations illustrate the versatility of this concept:

Aromatic Ketone Reduction. Hyster and co-workers (2019) reported the first radical-type enantioselective reduction of aromatic ketones **148** by merging a ruthenium photoredox catalyst with EREDs (Scheme 21a).[101] Ketone binding in the active site both attenuated its reduction potential—facilitating SET from Ru(I)—and fixed the geometry of the resulting ketyl radical **150**. Enantioselective HAT from FMN_{hq} then converted these radicals into chiral alcohols **149** with moderate *ee*.

Vinyl Pyridine Reduction. Expanding this strategy, the same team extended photoredox–enzyme cooperativity to vinyl pyridines **151** (Scheme 21b). By matching substrate orientation with the enzyme's hydrogen-donating pocket, they achieved highly efficient radical hydrogenation and broadened the reactivity of FMN-dependent enzymes well beyond their native scope.[102]

Hydroamination of olefins. More recently, Hyster and colleagues showcased the first C–N bond-forming radical cyclization within EREDs (Scheme 21c).[103] Light-driven SET from $Ru(bpy)_3Cl_2$ to N-centered precursors **154** produced highly reactive nitrogen radicals **156** that cyclized intramolecularly to carbon radicals **157** confined in the active site. Stereocontrolled HAT from FMN_{hq} then furnished β-stereogenic lactams **155** with high selectivity, extending enzymatic radical chemistry to C–N bond construction.

Building on their prior work, the same group found that $Ru(bpy)_3^{2+}$ binds to ene-reductase, localizing α-amino radical formation through SET oxidation of amino acids near the active site.[104] Stereochemical studies revealed that the HAT from FMN_{hq} to the prochiral radical intermediate is the enantiodecisive step, enabling the redox-neutral decarboxylative coupling of amino acids with high enantioselectivity. In a more recent study, the same group achieved an intermolecular enantioselective anti-Markovnikov hydroarylation of olefins using heteroaryl halides via synergistic photoenzymatic catalysis.[105]

6.2.3. Photoassisted ERED Catalysis

Light excitation dramatically expands the redox reach of flavin-dependent ene-reductases (EREDs). Upon irradiation, the reduced flavin (FMN_{hq}/FMN_{sq}) or enzyme–substrate charge-transfer (CT) complexes can engage in SET, initiating radical formation directly within the protein pocket. The nascent radical intermediate remains tightly confined by enzyme–substrate interactions and is terminated by highly enantioselective HAT from FMN_{sq}. This light-enabled strategy has unlocked radical reactivity far beyond the native scope of EREDs, enabling C–C, C–N, and C–S bond formations under mild conditions. Several landmark demonstrations illustrate the versatility of this concept:

Radical Generation via SET Reduction

Hydroalkylation of Alkenes. Zhao's group reported that photoexcitation of an ERED–substrate EDA complex **161** triggers single-electron reduction of α-bromo carbonyl compounds **158**, generating α-acyl radicals **162** (Scheme 22a).[106] These radicals add to 1,1-disubstituted alkenes **159** to give γ-carbon radicals **163**, which are then enantioselectively quenched by HAT from FMN_{sq} to furnish γ-stereogenic carbonyl compounds **160** with > 99% *ee*.

In 2024, the same group developed a photoenzymatic strategy for remote stereocontrol, enabling the hydroalkylation of olefins with halomethyl azaarenes via a charge-transfer complex.[107] Furthermore, the Xu's group has

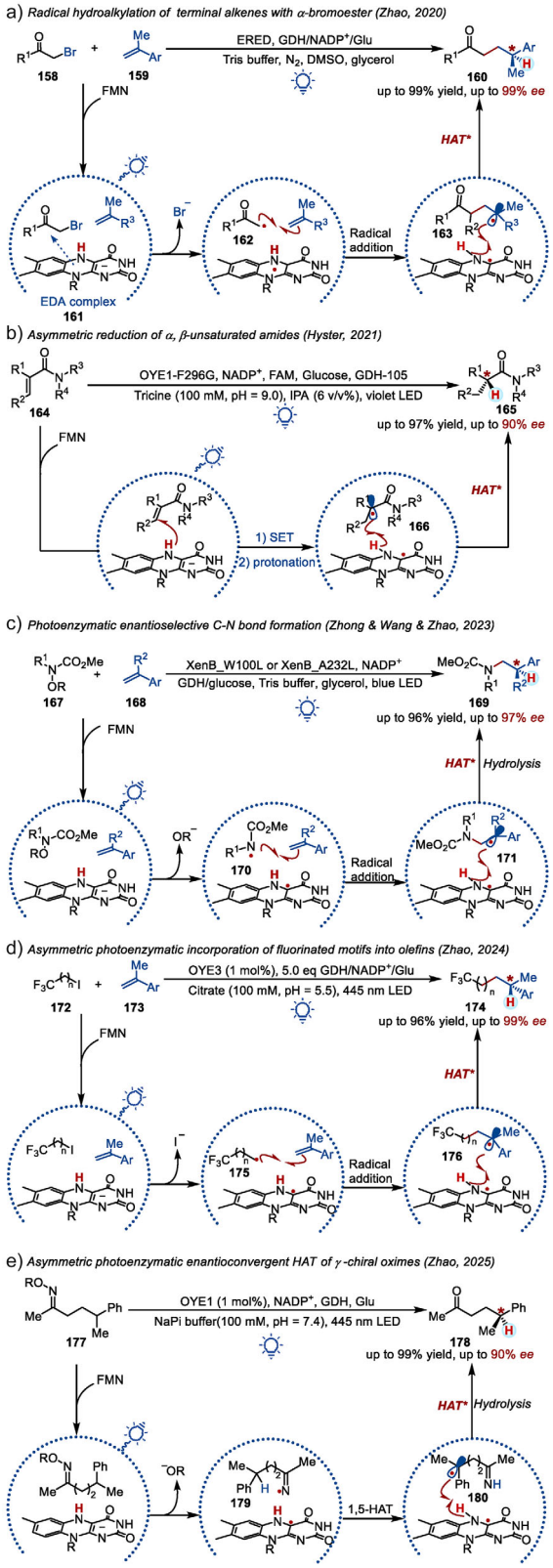

Scheme 22. Light-driven SET reduction in EREDs for asymmetric HAT. a) Intermolecular radical hydroalkylation of terminal alkenes and α-bromoester. b) Asymmetric reduction of α,β-unsaturated amides. c) Photoenzymatic enantioselective C—N bond formation. d) Asymmetric photoenzymatic incorporation of fluorinated motifs into olefins. e) Asymmetric photoenzymatic enantioconvergent HAT of γ-chiral oximes.

also leveraged the synergistic combination of light and enzymes to achieve enantioselective hydrodehalogenation of α,α-chlorofluoroketones[108] and hydrosulfonylation of aryl sulfonyl chlorides.[109]

Asymmetric Reduction of α,β-Unsaturated Amides. Direct excitation of FMN_{hq} produces a highly reducing singlet excited state that can deliver electrons to unactivated α,β-unsaturated amides **164** (Scheme 22b).[110] Protonation of the resulting radical anion, followed by stereoselective HAT from FMN_{sq}, generates α-stereogenic amides **165**.

Hydroamination of 1,1-Disubstituted Alkenes. Photoexcited EREDs generate amidyl radicals directly from protected primary aliphatic amines **167** bearing a labile N—O bond without any external photocatalyst. These nitrogen radicals **170** add to alkenes **168** and are subsequently hydrogenated enantioselectively via HAT by FMN_{hq}, producing optically enriched amines **169** (Scheme 22c).[111] In 2024, the same group achieved asymmetric hydroamination by extending the radical precursors from stable carbamates to notoriously reactive and difficult-to-control dialkyl amines, showcasing an advanced level of photoenzymatic mastery over complex radical intermediates.[112] Departing from prior approaches, in 2025, Huang leverages N-amidopyridinium salts as radical precursors activated by a green-light-absorbing organic dye in synergy with an ene-reductase, moving beyond native photoenzyme capabilities and enabling access to distinct nitrogen-containing architectures.[113]

Hydrofluoroalkylation of Alkenes. Iodofluoroalkanes **172** undergo photoinduced SET reduction and C—I cleavage within the ERED active site to yield fluoroalkyl radicals **175** (Scheme 22d).[114] Addition to vinyl arenes **173**, followed by FMN_{sq}-mediated HAT, provides fluoroalkylated products **174** with excellent enantioselectivity.

Stereoablative enantioconvergence of γ-chiral oximes. Photoexcitation of FMN_{hq} in ene-reductases enables single-electron reduction of γ-chiral oximes **177** to generate an iminyl radical **179** (Scheme 22e),[115] which undergoes stereoablative 1,5-HAT at a remote stereocenter. Subsequent enantioconvergent HAT from FMN_{sq} and hydrolysis yield γ-chiral ketones **178** with high enantioselectivity, achieving remote stereocontrol inaccessible to conventional catalysis.

Radical Generation via SET Oxidation

Hydroarylation of Alkenes. Visible-light excitation of the flavoprotein generates the oxidized flavin species, which oxidizes electron-rich arenes **181** to aryl cation radicals **184** (Scheme 23a). These activated arenes add to alkenes, and subsequent deprotonation restores aromaticity to give radical intermediates **185**. Enantioselective HAT from FMN_{sq} then terminates the radical, completing this redox-neutral hydroarylation and furnishing hydroarylated products **183** in high *ee*.[116]

Hydrosulfonylation of Alkenes. Single-electron oxidation of sulfonate salts **186** inside photoexcited EREDs generates sulfonyl radicals **189** that add to alkenes **187** (Scheme 23b).[117] The resulting prochiral radicals are captured by FMN_{sq}, forging C—S bonds and establishing the stereocenter of **188** with excellent enantioselectivity under mild aqueous conditions. Meanwhile, Xu and his co-workers

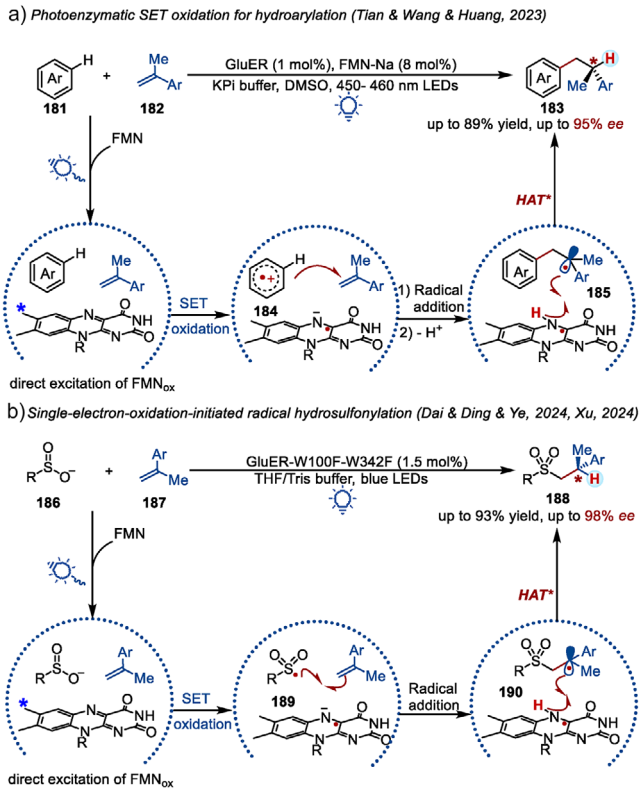

Scheme 23. Light-driven SET oxidation in EREDs for asymmetric HAT. a) Photoenzymatic SET oxidation for hydroarylation. b) Single-electron-oxidation-initiated radical hydrosulfonylation.

developed a redox-neutral photoenzymatic hydrosulfonylation using engineered OYE1. Initiated by photoexcited FMN, the reaction proceeds via a sulfonyl radical, with enantioselectivity determined by stereocontrolling HAT from FMN_{sq} to yield (*R*)-*β*-chiral sulfones **188**.[118]

7. Conclusion and Outlook

Viewed through the lens of where enantioselection is set, asymmetric HAT has evolved from a small collection of isolated examples into a coherent mechanistic landscape spanning five regimes—donation-controlled termination, radical-centered control, abstraction-controlled HAT, cooperative bimetallic systems, and enzyme-based platforms. Across these modes, a common theme emerges: Stereocontrol arises when radical generation, substrate confinement, and H-atom delivery are coordinated within a single organized manifold. The preceding sections outline how the field has gradually progressed from simple chiral donors to complex catalytic architectures capable of positioning radicals within well-defined chiral environments. Building on these developments, several avenues appear particularly promising (Figure 3).

i) **Catalyst Development — Toward Cooperative and Multinuclear Manifolds**

Transition-metal catalysis has already shown that metals such as Ti, Co, and Mn can couple radical generation with enantioselective HAT within a single catalytic manifold—an approach highlighted throughout this review. More recently, cooperative bimetallic systems have demonstrated that two metals acting in concert can further restrict radical diffusion and better align donor and acceptor geometries. Extending this logic, dinuclear or multinuclear architectures capable of integrating radical generation, binding, and stereocontrolled H-delivery in one confined pocket represent a natural next step, minimizing entropic penalties and offering broader reactivity and higher stereoselectivity. Hybrid approaches that position metal centers within peptide or protein frameworks may also provide enzyme-like control while maintaining the tunability of small-molecule catalysts. These strategies offer a path toward increasingly well-organized and stereoselective HAT catalysts capable of supporting broader and more demanding transformations.

ii) **Donor Development — Beyond Classical Low-BDE Reagents**

Donor-controlled asymmetric HAT remains dominated by thiols, nicotinamides, and tin/germanium reagents. However, several emerging designs highlight the potential for diversification. Imidazole, for instance, has recently been recognized as an unconventional H-atom donor in asymmetric HAT through a distinct coordination-enabled mechanism, underscoring the opportunity to exploit new donor manifolds. Moving forward, donors that are modular, sustainable, and tunable in both BDE and polarity will be essential. Simple feedstocks—water, alcohols, amines—remain largely unexplored; strategies such as polarity reversal catalysis or transient bond-weakening[119] could transform them into effective chiral donors. Equally important will be catalytic donor regeneration, which has already proven feasible in selected thiol systems and should become routine in future designs.

iii) **Activation Modes — Thermal, Photochemical, and Electrochemical Synergy**

As described in earlier sections, the activation landscape has expanded from classical thermochemistry to photochemical and enzymatic platforms capable of generating radicals under exceptionally mild conditions. Looking ahead, photoelectrochemical approaches offer an appealing hybrid mode: light can modulate selectivity and excited-state interactions, while electrochemistry can regenerate donors or define redox events with precision.[120–123] Such energy-efficient, reagent-economical methods could enable asymmetric HAT at late stages and in highly functionalized molecular settings.

iv) **Complex Molecules and Late-Stage Applications**

Beyond isotopic labeling and C─H editing, asymmetric radical cascades are beginning to appear in natural product settings. For example, Maimone and co-workers recently achieved enantioselective sesterterpene synthesis through a PRC-enabled radical cascade, illustrating how chiral H-atom delivery can be embedded within multi-bond-forming sequences. We anticipate that asymmetric HAT—whether donor-controlled, radical-centered, or enzyme-based—will find increasing use in the synthesis, modification, and diversification of bioactive molecules, agrochemicals, and functional materials.

As catalyst platforms move toward greater confinement, cooperation, and sustainability, the guiding question posed

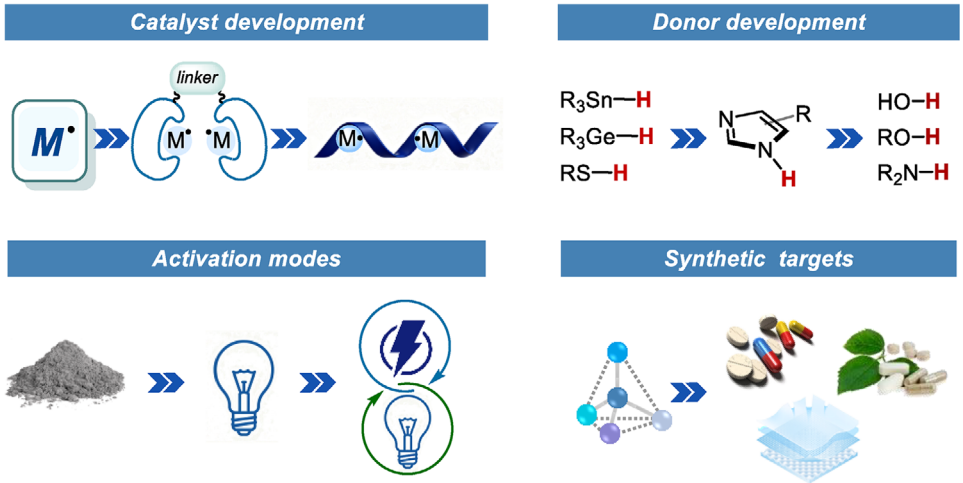

Figure 3. Strategic perspectives for asymmetric HAT development.

in this review—"Where is enantioselection set?"—should remain a practical compass for reaction design. Whether stereocontrol is encoded in the hydrogen donor, in a radical-binding environment, in the abstraction event, or in an integrated cycle that unifies these elements, this mechanistic map provides a foundation for rational catalyst planning. We anticipate that continued advances will bring asymmetric HAT closer to enzyme-like selectivity and efficiency, enabling greener, more precise, and more sustainable radical transformations in complex molecular settings.

Acknowledgements

Financial support from the National Natural Science Foundation of China (22371168), Natural Science Foundation of Shandong Province (ZR2023MB014), Natural Science Foundation of Shandong Province for Distinguished Young Scholars (ZR2025QA06), Shenzhen Science and Technology Innovation Program (JCYJ20230807094114030), and the Taishan Scholars Program of Shandong Province (tstp20250517) is greatly appreciated.

Conflict of Interests

The authors declare no conflict of interest.

Data Availability Statement

Data sharing is not applicable to this article as no new data were created or analyzed in this study.

Keywords: Asymmetric catalysis · Enantiocontrol · Hydrogen-atom transfer · Radical chemistry

[1] J. M. Mayer, *Acc. Chem. Res.* **2011**, *44*, 36–46, https://doi.org/10.1021/ar100093z.
[2] A. Studer, D. P. Curran, *Angew. Chem. Int. Ed.* **2016**, *55*, 58–102, https://doi.org/10.1002/anie.201505090.
[3] J. W. Darcy, B. Koronkiewicz, G. A. Parada, J. M. Mayer, *Acc. Chem. Res.* **2018**, *51*, 2391–2399, https://doi.org/10.1021/acs.accounts.8b00319.
[4] L. Capaldo, D. Ravelli, *Eur. J. Org. Chem.* **2017**, *2017*, 2056–2071, https://doi.org/10.1002/ejoc.201601485.
[5] Y. Nakano, K. F. Biegasiewicz, T. K. Hyster, *Curr. Opin. Chem. Biol.* **2019**, *49*, 16–24, https://doi.org/10.1016/j.cbpa.2018.09.001.
[6] H. Cao, X. Tang, H. Tang, Y. Yuan, J. Wu, *Chem. Catal.* **2021**, *1*, 523–598.
[7] Z. Ye, Y.-M. Lin, L. Gong, *Eur. J. Org. Chem.* **2021**, *2021*, 5545–5556, https://doi.org/10.1002/ejoc.202101036.
[8] L. Chang, S. Wang, Q. An, L. Liu, H. Wang, Y. Li, K. Feng, Z. Zuo, *Chem. Sci.* **2023**, *14*, 6841–6859, https://doi.org/10.1039/D3SC01118F.
[9] L. Capaldo, D. Ravelli, M. Fagnoni, *Chem. Rev.* **2022**, *122*, 1875–1924, https://doi.org/10.1021/acs.chemrev.1c00263.
[10] C. Yang, S. Arora, S. Maldonado, D. A. Pratt, C. R. J. Stephenson, *Nat. Rev. Chem.* **2023**, *7*, 653–666, https://doi.org/10.1038/s41570-023-00511-z.
[11] M. Yan, J. C. Lo, J. T. Edwards, P. S. Baran, *J. Am. Chem. Soc.* **2016**, *138*, 12692–12714, https://doi.org/10.1021/jacs.6b08856.
[12] D. A. Nagib, *Chem. Rev.* **2022**, *122*, 15989–15992, https://doi.org/10.1021/acs.chemrev.2c00622.
[13] M. Nechab, S. Mondal, M. P. Bertrand, *Chem. - Eur. J.* **2014**, *20*, 16034–16059, https://doi.org/10.1002/chem.201403951.
[14] L. M. Stateman, K. M. Nakafuku, D. A. Nagib, *Synth.* **2018**, *50*, 1569–1586.
[15] G. Kumar, S. Pradhan, I. Chatterjee, *Chem. Asian J.* **2020**, *15*, 651–672, https://doi.org/10.1002/asia.201901744.
[16] S. Sarkar, K. P. S. Cheung, V. Gevorgyan, *Chem. Sci.* **2020**, *11*, 12974–12993, https://doi.org/10.1039/D0SC04881J.
[17] D. Zhang, X. Hui, C. Wu, Y. Zhu, *ChemCatChem* **2021**, *13*, 3370–3380, https://doi.org/10.1002/cctc.202100248.
[18] F. S. Meger, J. A. Murphy, *Molecules* **2023**. *28*. 6127, https://doi.org/10.3390/molecules28166127.
[19] Y. Ping, S. Xu, W. Kong, *Acc. Chem. Res.* **2025**, *58*, 2477–2495, https://doi.org/10.1021/acs.accounts.5c00355.

[20] Y. H. Miao Wang, P. Hu, *Chin. J. Org. Chem.* **2025**, *45*, 477, https://doi.org/10.6023/cjoc202407027.

[21] S. L. Shevick, C. V. Wilson, S. Kotesova, D. Kim, P. L. Holland, R. A. Shenvi, *Chem. Sci.* **2020**, *11*, 12401–12422, https://doi.org/10.1039/D0SC04112B.

[22] S. Jana, V. J. Mayerhofer, C. J. Teskey, J. Christopher, *Angew. Chem. Int. Ed.* **2023**, *62*, e202304882.

[23] K. Mukherjee, A. Ben David, H. Nikoghosyan, R. Hakobyan, V. Gevorgyan, *Nat. Catal.* **2025**, *8*, 1146–1158, https://doi.org/10.1038/s41929-025-01431-5.

[24] M. P. Sibi, N. A. Porter, *Acc. Chem. Res.* **1999**, *32*, 163–171, https://doi.org/10.1021/ar9600547.

[25] J. Zimmerman, M. P. Sibi, in *Radicals in Synthesis I* (Ed.: A. Gansäuer), Springer Berlin Heidelberg, Berlin, Heidelberg, **2006**, pp. 107–162.

[26] H. Subramanian, M. P. Sibi, *Asian J. Org. Chem.* **2023**, *12*, e202300175.

[27] X. Han, C. He, *Chin. J. Chem.* **2024**, *42*, 3414–3428, https://doi.org/10.1002/cjoc.202400296.

[28] Y. Liu, Z. Yin, X. Yang, J. Cheng, *Chin. Chem. Lett.* **2025**, *36*, 110521, https://doi.org/10.1016/j.cclet.2024.110521.

[29] D. D. Tanner, A. Kharrat, *J. Am. Chem. Soc.* **1988**, *110*, 2968–2970, https://doi.org/10.1021/ja00217a046.

[30] A. Davies, *J. Chem. Res.* **2006**, *2006*, 141–148, https://doi.org/10.3184/030823406776330710.

[31] D. Nanni, D. P. Curran, *Tetrahedron: Asymmetry* **1996**, *7*, 2417–2422, https://doi.org/10.1016/0957-4166(96)00300-X.

[32] M. Blumenstein, K. Schwarzkopf, J. O. Metzger, *Angew. Chem. lnt. Ed.* **1997**, *36*, 235–236, https://doi.org/10.1002/anie.199702351.

[33] K. Ja-Hyo, K. Tae-Hyung, *Bull. Korean Chem. Soc.* **2003**, *24*, 1055–1056.

[34] D. Dakternieks, V. T. Perchyonok, C. H. Schiesser, *Tetrahedron: Asymmetry* **2003**, *14*, 3057–3068, https://doi.org/10.1016/j.tetasy.2003.07.012.

[35] G. Gualtieri, S. J. Geib, D. P. Curran, *J. Org. Chem.* **2003**, *68*, 5013–5019, https://doi.org/10.1021/jo026625s.

[36] L. Zeng, V. T. Perchyonok, C. H. Schiesser, *Tetrahedron: Asymmetry* **2004**, *15*, 2547–2554, https://doi.org/10.1016/j.tetasy.2004.06.020.

[37] B. P. Roberts, *Chem. Soc. Rev.* **1999**, *28*, 25–35, https://doi.org/10.1039/a804291h.

[38] F. Parsaee, M. C. Senarathna, P. B. Kannangara, S. N. Alexander, P. D. E. Arche, E. R. Welin, *Nat. Rev. Chem.* **2021**, *5*, 486–499, https://doi.org/10.1038/s41570-021-00284-3.

[39] Y. Cai, B. P. Roberts, D. A. Tocher, *J. Chem. Soc., Perkin Trans.* **2002**, *1*, 1376–1386, https://doi.org/10.1039/b202022j.

[40] Z. G. Brill, H. K. Grover, T. J. Maimone, *Science* **2016**, *352*, 1078–1082, https://doi.org/10.1126/science.aaf6742.

[41] N. Y. Shin, J. M. Ryss, X. Zhang, S. J. Miller, R. R. Knowles, *Science* **2019**, *366*, 364–369, https://doi.org/10.1126/science.aay2204.

[42] B. G. Hejna, J. M. Ganley, H. Shao, H. Tian, J. D. Ellefsen, N. J. Fastuca, K. N. Houk, S. J. Miller, R. R. Knowles, *J. Am. Chem. Soc.* **2023**, *145*, 16118–16129, https://doi.org/10.1021/jacs.3c04591.

[43] M. V. Pinto Pereira Junior, E. P. Geunes, H. Shao, Y. Zhang, J. Cheng, S. V. Magpantay, B. Q. Mercado, J. M. Mayer, K. N. Houk, R. R. Knowles, S. J. Miller, *J. Am. Chem. Soc.* **2025**, *147*, 11412–11424, https://doi.org/10.1021/jacs.5c01166.

[44] Q. Shi, M. Xu, R. Chang, D. Ramanathan, B. Peñin, I. Funes-Ardoiz, J. Ye, *Nat. Commun.* **2022**, *13*, 4453, https://doi.org/10.1038/s41467-022-32238-8.

[45] X. Yan, Y. Pang, Y. Zhou, R. Chang, J. Ye, *J. Am. Chem. Soc.* **2025**, *147*, 1186–1196, https://doi.org/10.1021/jacs.4c14934.

[46] L. Tang, C. Shen, S. Hao, K. Dong, *J. Am. Chem. Soc.* **2024**, *146*, 16248–16256, https://doi.org/10.1021/jacs.4c04596.

[47] Y. Xu, C. Shen, K. Dong, *J. Am. Chem. Soc.* **2025**, *147*, 6259–6267, https://doi.org/10.1021/jacs.4c18464.

[48] L. Li, S.-q. Zhang, X. Cui, G. Zhao, Z. Tang, G.-x. Li, *Org. Lett.* **2024**, *26*, 8371–8376, https://doi.org/10.1021/acs.orglett.4c03175.

[49] Y. Luo, Q. Wei, L. Yang, Y. Zhou, W. Cao, Z. Su, X. Liu, X. Feng, *ACS Catal.* **2022**, *12*, 12984–12992, https://doi.org/10.1021/acscatal.2c04047.

[50] Y. Luo, Y. Zhou, F. Xiao, X. He, Z. Zhong, Q.-L. Zhou, W. Cao, X. Liu, X. Feng, *ACS Catal.* **2024**, *14*, 12031–12041, https://doi.org/10.1021/acscatal.4c03512.

[51] M. P. Sibi, Y. Asano, J. B. Sausker, *Angew. Chem. Int. Ed.* **2001**, *40*, 1293–1296, https://doi.org/10.1002/1521-3773(20010401)40:7⟨1293::AID-ANIE1293⟩3.0.CO;2-Y.

[52] M. P. Sibi, K. Patil, *Angew. Chem. Int. Ed.* **2004**, *43*, 1235–1238, https://doi.org/10.1002/anie.200353000.

[53] M. P. Sibi, K. Patil, *Org. Lett.* **2005**, *7*, 1453–1456, https://doi.org/10.1021/ol047347h.

[54] H. Sugimoto, S. Nakamura, Y. Watanabe, T. Toru, *Tetrahedron: Asymmetry.* **2003**, *14*, 3043–3055.

[55] M. P. Sibi, S. Nad, *Angew. Chem. Int. Ed.* **2007**, *46*, 9231–9234, https://doi.org/10.1002/anie.200702976.

[56] A. Gansäuer, M. Klatte, G. M. Brändle, J. Friedrich, *Angew. Chem. Int. Ed.* **2012**, *51*, 8891–8894, https://doi.org/10.1002/anie.201202818.

[57] D. S. G. Henriques, E. Rojo-Wiechel, S. Klare, R. Mika, S. Höthker, J. H. Schacht, N. Schmickler, A. Gansäuer, *Angew. Chem. Int. Ed.* **2022**, *61*, e202114198, https://doi.org/10.1002/anie.202114198.

[58] Z. Xu, J. Shen, L. Li, W. Chen, S. Li, J. Jiang, Y.-Q. Zhang, *Angew. Chem. Int. Ed.* **2023**, *61*, e202214111.

[59] T. Aechtner, M. Dressel, T. Bach, *Angew. Chem. Int. Ed.* **2004**, *43*, 5849–5851.

[60] J. Großkopf, Plaza, M. A. S., S. Breitenlechner, G. Storch, T. Bach, *J. Am. Chem. Soc.* **2021**, *143*, 21241–21245.

[61] J. Großkopf, A. A. Heidecker, T. Bach, *Angew. Chem. Int. Ed.* **2023**, *135*, e202305274.

[62] J. Großkopf, M. Plaza, R. J. Kutta, P. Nuernberger, T. Bach, *Angew. Chem. Int. Ed.* **2023**, *62*, e202313606.

[63] M. Iglhaut, P. Freund, T. Bach, *Angew. Chem. Int. Ed.* **2025**, *64*, e202418873.

[64] P. Freund, M. Pauls, D. Babushkina, T. Pickl, C. Bannwarth, T. Bach, *J. Am. Chem. Soc.* **2025**, *147*, 1434–1439, https://doi.org/10.1021/jacs.4c16053.

[65] C. Zhou, T. Bach, *J. Am. Chem. Soc.* **2025**, *147*, 25148–25152, https://doi.org/10.1021/jacs.5c07524.

[66] P. L. H. Mok, B. P. Roberts, *J. Chem. Soc., Chem. Commun. 0*, 150–152, https://doi.org/10.1039/C39910000150.

[67] P. L. H. Mok, B. P. Roberts, *Tetrahedron Lett.* **1992**, *33*, 7249–7252, https://doi.org/10.1016/S0040-4039(00)60885-7.

[68] P. L. H. Mok, B. P. Roberts, P. T. McKetty, *J. Chem. Soc., Perkin Trans. 2* **1993**, 665–674, https://doi.org/10.1039/P29930000665.

[69] H.-S. Dang, V. Diart, B. P. Roberts, D. A. Tocher, *J. Chem. Soc., Perkin Trans. 2* **1994**, 1039–1045, https://doi.org/10.1039/P29940001039.

[70] H.-S. Dang, B. P. Roberts, *Tetrahedron Lett.* **1995**, *36*, 3731–3734, https://doi.org/10.1016/0040-4039(95)00566-U.

[71] M. Cao, H. Wang, F. Hou, Y. Zhu, Q. Liu, C.-H. Tung, L. Liu, *J. Am. Chem. Soc.* **2024**, *146*, 18396–18406, https://doi.org/10.1021/jacs.4c03610.

[72] S. Sun, Y. Yang, R. Zhao, D. Zhang, L. Liu, *J. Am. Chem. Soc.* **2020**, *142*, 19346–19353, https://doi.org/10.1021/jacs.0c09636.

[73] S. Sun, Y. Ma, Z. Liu, L. Liu, *Angew. Chem. Int. Ed.* **2021**, *60*, 176–180, https://doi.org/10.1002/anie.202009594.

[74] P. Ye, A. Feng, L. Wang, M. Cao, R. Zhu, L. Liu, *Nat. Commun.* **2022**, *13*, 1621, https://doi.org/10.1038/s41467-022-29319-z.

[75] M. Kuroboshi, H. Yoshihisa, M. N. Cortona, Y. Kawakami, Z. Gao, H. Tanaka, *Tetrahedron Lett.* **2000**, *41*, 8131–8135, https://doi.org/10.1016/S0040-4039(00)01419-2.

[76] M. Nechab, D. N. Kumar, C. Philouze, C. Einhorn, J. Einhorn, *Angew. Chem. Int. Ed.* **2007**, *46*, 3080–3083, https://doi.org/10.1002/anie.200603780.

[77] A. S. K. Lahdenperä, J. Dhankhar, D. J. Davies, N. Y. S. Lam, P. D. Bacoş, K. de la Vega-Hernández, R. J. Phipps, *Science* **2024**, *386*, 42–49, https://doi.org/10.1126/science.adq8029.

[78] N. Y. S. Lam, J. Dhankhar, A. S. K. Lahdenperä, R. J. Phipps, *J. Am. Chem. Soc.* **2024**, *146*, 33302–33308, https://doi.org/10.1021/jacs.4c13919.

[79] A. Miyafuji, T. Katsuki, *Tetrahedron* **1998**, *54*, 10339–10348, https://doi.org/10.1016/S0040-4020(98)00489-X.

[80] M. Milan, M. Bietti, M. Costas, *ACS Cent. Sci.* **2017**, *3*, 196–204, https://doi.org/10.1021/acscentsci.6b00368.

[81] A. Palone, G. Casadevall, S. Ruiz-Barragan, A. Call, S. Osuna, M. Bietti, M. Costas, *J. Am. Chem. Soc.* **2023**, *145*, 15742–15753, https://doi.org/10.1021/jacs.2c10148.

[82] A. Call, G. Capocasa, A. Palone, L. Vicens, E. Aparicio, N. Choukairi Afailal, N. Siakavaras, M. E. López Saló, M. Bietti, M. Costas, *J. Am. Chem. Soc.* **2023**, *145*, 18094–18103, https://doi.org/10.1021/jacs.3c06231.

[83] K. Lang, S. Torker, L. Wojtas, X. P. Zhang, *J. Am. Chem. Soc.* **2019**, *141*, 12388–12396, https://doi.org/10.1021/jacs.9b05850.

[84] K. Lang, Y. Hu, W.-C. C. Lee, X. P. Zhang, *Nat. Synth.* **2022**, *1*, 548–557, https://doi.org/10.1038/s44160-022-00107-3.

[85] W.-C. C. Lee, D.-S. Wang, A. Deb, Y. Zhu, X. P. Zhang, *J. Am. Chem. Soc.* **2025**, *147*, 24001–24013, https://doi.org/10.1021/jacs.5c07473.

[86] Y. Liu, B. Yang, H. He, S. Gao, *Angew. Chem. Int. Ed.* **2025**, *64*, e202516814.

[87] J. Shen, F. Wang, Z. Ma, J. Jiang, Y.-Q. Zhang, *J. Am. Chem. Soc.* **2025**, *147*, 27224–27231, https://doi.org/10.1021/jacs.5c10189.

[88] M. A. Emmanuel, S. G. Bender, C. Bilodeau, J. M. Carceller, J. S. DeHovitz, H. Fu, Y. Liu, B. T. Nicholls, Y. Ouyang, C. G. Page, T. Qiao, F. C. Raps, D. R. Sorigué, S.-Z. Sun, J. Turek-Herman, Y. Ye, A. Rivas-Souchet, J. Cao, T. K. Hyster, *Chem. Rev.* **2023**, *123*, 5459–5520, https://doi.org/10.1021/acs.chemrev.2c00767.

[89] E. García-Urdiales, I. Lavandera, V. Gotor, in *Enzyme Catalysis in Organic Synthesis*, 3rd ed. (Eds.: K. Drauz, H. Gröger and O. May), Wiley-VCH, Weinheim **2012**, pp. 43–66.

[90] H. S. Toogood, N. S. Scrutton, *ACS Catal.* **2018**, *8*, 3532–3549, https://doi.org/10.1021/acscatal.8b00624.

[91] H. Fu, T. K. Hyster, *Acc. Chem. Res.* **2024**, *57*, 1446–1457, https://doi.org/10.1021/acs.accounts.4c00129.

[92] L. S. Vidal, C. L. Kelly, P. M. Mordaka, J. T. Heap, *Bba-proteins Proteom* **2018**, *1866*, 327–347, https://doi.org/10.1016/j.bbapap.2017.11.005.

[93] R. Miura, *Chem. Rec.* **2001**, *1*, 183–194, https://doi.org/10.1002/tcr.1007.

[94] K. F. Biegasiewicz, S. J. Cooper, M. A. Emmanuel, D. C. Miller, T. K. Hyster, *Nat. Chem.* **2018**, *10*, 770–775, https://doi.org/10.1038/s41557-018-0059-y.

[95] M. A. Emmanuel, N. R. Greenberg, D. G. Oblinsky, T. K. Hyster, *Nature* **2016**, *540*, 414–417, https://doi.org/10.1038/nature20569.

[96] X. Huang, J. Feng, J. Cui, G. Jiang, W. Harrison, X. Zang, J. Zhou, B. Wang, H. Zhao, *Nat. Catal.* **2022**, *5*, 586–593, https://doi.org/10.1038/s41929-022-00777-4.

[97] B. Chen, R. Li, J. Feng, B. Zhao, J. Zhang, J. Yu, Y. Xu, Z. Xing, Y. Zhao, B. Wang, X. Huang, *J. Am. Chem. Soc.* **2024**, *146*, 14278–14286, https://doi.org/10.1021/jacs.4c03879.

[98] B. A. Sandoval, A. J. Meichan, T. K. Hyster, *J. Am. Chem. Soc.* **2017**, *139*, 11313–11316, https://doi.org/10.1021/jacs.7b05468.

[99] B. Chen, Q. Zhang, J. Yu, B. Zhao, R. Ge, Z. Zhang, D. Luo, B. Wang, X. Huang, *Nat. Catal.* **2025**, *8*, 740–748, https://doi.org/10.1038/s41929-025-01372-z.

[100] X. Duan, D. Cui, M. Wang, C. Jin, X. Cai, Z. Wang, J. Xu, *Nat. Commun.* **2025**, *16*, 1225, https://doi.org/10.1038/s41467-025-56437-1.

[101] B. A. Sandoval, S. I. Kurtoic, M. M. Chung, K. F. Biegasiewicz, T. K. Hyster, *Angew. Chem. Int. Ed.* **2019**, *58*, 8714–8718, https://doi.org/10.1002/anie.201902005.

[102] Y. Nakano, M. J. Black, A. J. Meichan, B. A. Sandoval, M. M. Chung, K. F. Biegasiewicz, T. Zhu, T. K. Hyster, *Angew. Chem. Int. Ed.* **2020**, *59*, 10484–10488, https://doi.org/10.1002/anie.202003125.

[103] Y. Ye, J. Cao, D. G. Oblinsky, D. Verma, C. K. Prier, G. D. Scholes, T. K. Hyster, *Nat. Chem.* **2023**, *15*, 206–212, https://doi.org/10.1038/s41557-022-01083-z.

[104] S.-Z. Sun, B. T. Nicholls, D. Bain, T. Qiao, C. G. Page, A. J. Musser, T. K. Hyster, *Nat. Catal.* **2024**, *7*, 35–42, https://doi.org/10.1038/s41929-023-01065-5.

[105] P. Mukherjee, Z. Alassad, T. K. Hyster, *J. Am. Chem. Soc.* **2025**, *147*, 14048–14053, https://doi.org/10.1021/jacs.5c01066.

[106] X. Huang, B. Wang, Y. Wang, G. Jiang, J. Feng, H. Zhao, *Nature* **2020**, *584*, 69–74, https://doi.org/10.1038/s41586-020-2406-6.

[107] M. Li, W. Harrison, Z. Zhang, Y. Yuan, H. Zhao, *Nat. Chem.* **2024**, *16*, 277–284, https://doi.org/10.1038/s41557-023-01368-x.

[108] Y. Peng, Z. Wang, Y. Chen, W. Xu, Y. Hu, Z. Chen, J. Xu, Q. Wu, *Angew. Chem. Int. Ed.* **2022**, *61*, e202211199, https://doi.org/10.1002/anie.202211199.

[109] X. Chen, D. Zheng, L. Jiang, Z. Wang, X. Duan, D. Cui, S. Liu, Y. Zhang, X. Yu, J. Ge, J. Xu, *Angew. Chem. Int. Ed.* **2023**, *62*, e202218140, https://doi.org/10.1002/anie.202218140.

[110] B. A. Sandoval, P. D. Clayman, D. G. Oblinsky, S. Oh, Y. Nakano, M. Bird, G. D. Scholes, T. K. Hyster, *J. Am. Chem. Soc.* **2021**, *143*, 1735–1739, https://doi.org/10.1021/jacs.0c11494.

[111] Z. Zhang, J. Feng, C. Yang, H. Cui, W. Harrison, D. Zhong, B. Wang, H. Zhao, *Nat. Catal.* **2023**, *6*, 687–694, https://doi.org/10.1038/s41929-023-00994-5.

[112] W. Harrison, G. Jiang, Z. Zhang, M. Li, H. Chen, H. Zhao, *J. Am. Chem. Soc.* **2024**, *146*, 10716–10722, https://doi.org/10.1021/jacs.4c00620.

[113] F. Shi, B. Chen, J. Yu, R. Zhu, Y. Zheng, X. Huang, *Chin. J. Catal.* **2025**, *68*, 223–229, https://doi.org/10.1016/S1872-2067(24)60168-3.

[114] M. Li, Y. Yuan, W. Harrison, Z. Zhang, H. Zhao, *Science* **2024**, *385*, 416–421, https://doi.org/10.1126/science.adk8464.

[115] Z. Zhang, M. Li, W. Harrison, J. Lu, Z. Zhao, Y. Yuan, H. Zhao, *Nat. Catal.* **2025**, *8*, 548–555, https://doi.org/10.1038/s41929-025-01347-0.

[116] B. Zhao, J. Feng, L. Yu, Z. Xing, B. Chen, A. Liu, F. Liu, F. Shi, Y. Zhao, C. Tian, B. Wang, X. Huang, *Nat. Catal.* **2023**, *6*, 996–1004, https://doi.org/10.1038/s41929-023-01024-0.

[117] Q. Shi, X.-W. Kang, Z. Liu, P. Sakthivel, H. Aman, R. Chang, X. Yan, Y. Pang, S. Dai, B. Ding, J. Ye, *J. Am. Chem. Soc.* **2024**, *146*, 2748–2756, https://doi.org/10.1021/jacs.3c12513.

[118] L. Jiang, D. Zheng, X. Chen, D. Cui, X. Duan, Z. Wang, J. Ge, J. Xu, *ACS Catal.* **2024**, *14*, 6710–6716, https://doi.org/10.1021/acscatal.4c00350.

[119] N. G. Boekell, R. A. Flowers, *Chem. Rev.* **2022**, *122*, 13447–13477, https://doi.org/10.1021/acs.chemrev.2c00254.

[120] M. Yan, Y. Kawamata, P. S. Baran, *Chem. Rev.* **2017**, *117*, 13230–13319, https://doi.org/10.1021/acs.chemrev.7b00397.

[121] M. Ghosh, V. S. Shinde, M. Rueping, *Beilstein J. Org. Chem.* **2019**, *15*, 2710–2746, https://doi.org/10.3762/bjoc.15.264.

[122] J. Rein, S. B. Zacate, K. Mao, S. Lin, *Chem. Soc. Rev.* **2023**, *52*, 8106–8125, https://doi.org/10.1039/D3CS00511A.
[123] S. Zhang, M. Findlater, *ACS Catal.* **2023**, *13*, 8731–8751, https://doi.org/10.1021/acscatal.3c01221.

Manuscript received: December 08, 2025
Revised manuscript received: January 13, 2026
Manuscript accepted: January 13, 2026
Version of record online: ■■, ■■